# Integrative genomics identifies lncRNA regulatory networks across 1,044 pediatric leukemias and extra-cranial solid tumors

Apexa Modi[1,2], Gonzalo Lopez[1], Karina L. Conkrite[1], Chun Su[3], Tsz Ching Leung[1], Sathvik Ramanan[1], Elisabetta Manduchi[3], Matthew E. Johnson[3], Daphne Cheung[1], Samantha Gadd[4], Jinghui Zhang[5], Malcolm A. Smith[6], Jaime M. Guidry Auvil[7], Daniela S. Gerhard[6], Soheil Meshinchi[8], Elizabeth J. Perlman[4], Stephen P. Hunger[1,9], John M. Maris[1,9,11], Andrew D. Wells[3,11], Struan F.A. Grant[3,9,12,13], Sharon J. Diskin[1,9,10*]

[1] Division of Oncology and Center for Childhood Cancer Research, Children's Hospital of Philadelphia, Philadelphia, Pennsylvania 19104, USA.

[2] Genomics and Computational Biology Graduate Group, Biomedical Graduate Studies, Perelman School of Medicine, University of Pennsylvania, Philadelphia, Pennsylvania 19104, USA.

[3] Center for Spatial and Functional Genomics, Children's Hospital of Philadelphia, Philadelphia, Pennsylvania, USA.

[4] Department of Pathology and Laboratory Medicine, Ann & Robert H. Lurie Children's Hospital of Chicago, Robert H. Lurie Cancer Center, Northwestern University, Chicago, Illinois 60208, USA.

[5] Department of Computational Biology, St Jude Children's Research Hospital, Memphis, Tennessee 38105, USA

[6] Cancer Therapy Evaluation Program, National Cancer Institute, Bethesda, Maryland 20892, USA.

[7] Office of Cancer Genomics, National Cancer Institute, Bethesda, Maryland 20892, USA.

[8] Clinical Research Division, Fred Hutchinson Cancer Research Center, Seattle, Washington 98109, USA.

[9] Department of Pediatrics, Perelman School of Medicine at the University of Pennsylvania, Philadelphia, Pennsylvania 19104, USA.

[10] Abramson Family Cancer Research Institute, Perelman School of Medicine at the University of Pennsylvania, Philadelphia, Pennsylvania 19104, USA.

[11] Department of Pathology and Laboratory Medicine, Perelman School of Medicine at the University of Pennsylvania, Philadelphia, Pennsylvania 19104, USA.

[12] Department of Genetics, Perelman School of Medicine at the University of Pennsylvania, Philadelphia, Pennsylvania 19104, USA.

[13] Divisions of Human Genetics and Endocrinology & Diabetes, Children's Hospital of Philadelphia, Philadelphia, Pennsylvania, 19104, USA.

* Corresponding Author: diskin@email.chop.edu

## Abstract

Long non-coding RNAs (lncRNAs) play an important role in gene regulation and contribute to tumorigenesis. While pan-cancer studies of lncRNA expression have been performed for adult malignancies, the lncRNA landscape across pediatric cancers remains largely uncharted. Here, we curate RNA sequencing data for 1,044 pediatric leukemia and solid tumors and integrate paired tumor whole genome sequencing and epigenetic data in relevant cell line models to explore lncRNA expression, regulation, and association with cancer. We report a total of 2,657 robustly expressed lncRNAs across six pediatric cancers, including 1,142 exhibiting histotype-specific expression. DNA copy number alterations contributed to lncRNA dysregulation at a proportion comparable to protein coding genes. Application of a multi-dimensional framework to identify and prioritize lncRNAs impacting gene networks revealed that lncRNAs dysregulated in pediatric cancer are associated with proliferation, metabolism, and DNA damage hallmarks. Analysis of upstream regulation via cell-type specific transcription factors further implicated distinct histotype-specific and developmental lncRNAs. We integrated our analyses to prioritize lncRNAs for experimental validation and showed that silencing of *TBX2-AS1*, our top-prioritized neuroblastoma-specific lncRNA, resulted in significant growth inhibition of neuroblastoma cells, confirming our computational predictions. Taken together, these data provide a comprehensive characterization of lncRNA regulation and function in pediatric cancers and pave the way for future mechanistic studies.

74 Long non-coding RNAs (lncRNAs) are transcribed RNA molecules greater than 200 nucleotides in length
75 that do not code for proteins. These molecules account for 70% of the expressed human transcriptome
76 and provide a key aspect of gene regulation[1-4]. Compared to protein coding genes (PCGs), lncRNAs
77 typically have fewer exons, weaker conservation, and lower abundance[3]. Despite this, lncRNAs have
78 been shown to play significant roles in both transcriptional and post-transcriptional gene regulation[5].
79 LncRNAs perform these roles by physically interacting with a variety of substrates, including proteins
80 (transcription co-factors), RNAs (microRNA sponges), and DNA (chromatin interaction scaffolds)[1,2,6,7].
81 While the mechanisms and function for the majority of lncRNAs remain unknown[3,8], those that have been
82 experimentally characterized are involved in a variety of cellular processes[6] including gene silencing
83 (*ANRIL*)[9], modulation of chromatin architecture (*Xist*)[10], and pre-mRNA processing (*MALAT1*)[11].
84 LncRNAs are also important in development[12]. For example, the *H19* lncRNA is involved in imprinting[13],
85 while the well-conserved *TUNA* lncRNA controls stem cell pluripotency and lineage differentiation[14].
86 Dysregulation of lncRNA expression has been widely observed in cancer[3,15,16] and studies have
87 shown that lncRNAs play important roles in tumor initiation and progression[17]. LncRNAs can function as
88 tumor suppressors, such as the *PANDA* lncRNA which regulates DNA damage response in diffuse large
89 B-cell lymphoma[18]; however, many more lncRNAs appear to be oncogenes. Examples include the
90 *HOTAIR* and *PVT1* lncRNAs which promote proliferation in various cancers through tissue specific
91 mechanisms[19,20]. Pan-cancer analyses of lncRNA expression in adult malignancies have uncovered
92 many cancer-associated lncRNAs[3,15-17,21,22]. Identification of functional lncRNAs amongst the large set of
93 cancer-associated lncRNAs, however, remains challenging[15,23]. Current methods to identify putative
94 functional lncRNAs involve identifying lncRNA-specific genetic aberrations[15,16,24] or using lncRNA
95 expression to predict overall patient survival[16]. To more systematically address how lncRNAs drive the
96 pathogenesis of cancer, recent computational methods seek to assign function to these molecules based
97 on predicted target genes and regulatory network models. These methods have been applied to adult
98 malignancies and allow for more focused hypotheses to be tested[21,22].

99 LncRNA studies and evidence of related function in pediatric cancers have been primarily limited
100 to neuroblastoma (NBL)[25-30], T-lymphoblastic leukemia (T-ALL)[31,32], and more recently glioblastoma[33].
101 *CASC15* and *NBAT-1* are a sense-antisense lncRNA pair that map to a NBL susceptibility locus identified
102 by genome-wide association study[26,34]. Both lncRNAs are downregulated in high-risk NBL tumors and
103 have been shown to be involved in cell proliferation and differentiation[25,26]. In pediatric T-ALL, the
104 NOTCH-regulated lncRNA, *LUNAR1*, promotes T-ALL cell growth by sustaining IGF1 signaling[32]. To
105 date, it is unknown whether lncRNAs function as common drivers across multiple pediatric cancers, or if
106 instead, the majority of lncRNAs influence oncogenesis in a histotype-specific manner. Furthermore,
107 given that pediatric cancers typically arise from primitive embryonic and mesodermal cells, rather than
108 adult epithelial cells, it is unclear whether adult cancer lncRNA drivers will also be implicated in childhood
109 cancer.

110 Here, we perform a pan-pediatric cancer study of lncRNAs across 1,044 pediatric leukemias and
111 extra-cranial solid tumors[35,36]. We present the landscape of lncRNA expression across these childhood
112 cancers and perform integrative multi-omic analyses to assess tissue specificity, regulation, and putative
113 function. To validate our approach, we show that silencing of the top-prioritized NBL-specific
114 lncRNA, *TBX2-AS1*, impairs NBL cell growth in human-derived NBL cell line models.

115

116 ## Results

117 ### The lncRNA landscape of pediatric cancers

118 To define the repertoire of lncRNAs expressed in childhood cancers, we analyzed RNA-sequencing data
119 from six distinct pediatric cancer histotypes profiled through the Therapeutically Applicable Research to
120 Generate Effective Treatments (TARGET) project (https://ocg.cancer.gov/programs/target/data-matrix)
121 (**Online Methods; Supplementary Table 1).** This curated set of 1,044 leukemia and solid tumor samples
122 includes 280 acute myeloid leukemia (AML), 190 B-lymphoblastic leukemias (B-ALL), 244 T-
123 lymphoblastic leukemias (T-ALL), 121 Wilms tumors (WT), 48 extracranial rhabdoid tumors (RT), and
124 161 neuroblastomas (NBL) (**Fig. 1a**). Since one of our goals was to identify novel cancer-associated

125 lncRNAs, we performed guided *de novo* transcriptome assembly using StringTie v1.3.3[37] with the
126 GENCODE v19 database [38] as a gene annotation reference (**Supplementary Fig. 1**). Expressed gene
127 sequences that did not match exons and transcript structures of any known gene in the GENCODE v19
128 or RefSeq v74 databases were considered putative novel genes (**Supplementary Fig. 1, Online**
129 **Methods**). Of these novel genes, we identified candidate lncRNAs by using the PLEK v1 algorithm[39] to
130 assess non-coding potential, and then additionally filtered hits by transcript length, exon read coverage,
131 and genomic location (**Fig. 1a, Online Methods, Supplementary Fig. 1**). As validation of our lncRNA
132 discovery pipeline, we observed that 36% (87 of 242) of identified novel lncRNAs not annotated in
133 Gencode v19 (hg19) were indeed annotated in the more recent Gencode v29 (hg38) genome build
134 (**Supplementary Table 2**). To ensure that we selected robustly expressed genes in the setting of cancer
135 heterogeneity and sequencing variability, we applied a conservative expression cutoff of Fragments Per
136 Kilobase of transcript per Million mapped reads (FPKM) >1 in at least 20% of samples for each cancer.
137 Across all cancers there were 15,588 PCGs, 2,512 known lncRNAs, and 145 novel lncRNAs expressed,
138 though the total number of expressed genes varied per cancer (**Fig 1b, Supplementary Table 3**).
139 Principal component analysis (PCA) of lncRNA gene expression showed that blood (AML, B-ALL, T-ALL)
140 and solid (NBL, WT, RT) cancers form two distinct groups. Moreover, individual cancer histotypes
141 clustered more closely using lncRNA expression than PCG expression alone (**Supplementary Fig. 2a-**
142 **b**), consistent with the known tissue specific nature of lncRNA expression and function[3].

143 Overall, lncRNAs had lower average expression compared to PCGs resulting in fewer highly
144 expressed lncRNAs (**Supplementary Fig. 2c**). Between 10-100 (3.7%) lncRNAs accounted for 50% of
145 the total sum of lncRNA expression (**Fig. 1c**). In contrast, between 100-1000 (6.4%) PCGs accounted for
146 50% of the total sum of PCG expression (**Fig. 1d**). We examined the union of the top five most highly
147 expressed lncRNAs across pediatric cancers (total 11 lncRNAs). Some of these lncRNAs had higher
148 expression in the blood cancers (*MALAT1* and *RP11-386I14.4*), in the solid cancers (*H19)*, or in only one
149 cancer, such as *MEG3* and *RP11-386G11.10* in NBL (**Fig. 1e**). Five of these lncRNAs were among the
150 top 10 lncRNAs expressed across normal tissues in the Genotype-Tissue Expression (GTEx) project [40].

151 Specifically, *C17orf76-AS1 (LRRC75A-AS1), MALAT1, GAS5, SNHG6, SNHG8* were expressed
152 ubiquitously in 30 of the 49 GTEx tissues (**Supplementary Table 4**).
153
154 **Tissue specific lncRNA expression distinguishes pediatric cancers**
155 To evaluate more formally the tissue specific expression of lncRNAs, we annotated all genes with a tissue
156 specificity index (tau score)[41,42] (**Online Methods**). The established tau score ranges from 0 (ubiquitous
157 expression) to 1 (tissue-specific). As an example, the highly expressed lncRNA *C17orf76-AS1* yielded a
158 tau score of 0.296 in this study, indicating ubiquitous expression (**Supplementary Fig. 2d**). In contrast,
159 the highly expressed *MEG3* lncRNA, which is known to have tissue-specific expression in NBL[30,43],
160 yielded a tau score of 0.986 (**Supplementary Fig. 2e**). Overall, we observed that lncRNAs yielded a
161 higher tau score range and mean, and thus greater tissue specific expression than PCGs (t-test
162 $p=1.62x10^{-42}$). Novel lncRNAs had the greatest tissue specific expression (t-test: vs proteins- $p=1.62x10^{-}$
163 $^{42}$, vs known lncRNAs- $p = 3.39x10^{-13}$) (**Fig. 2a**). A tau score threshold of 0.8 has been suggested to
164 distinguish tissue specific genes[42], and using this cutoff we identified 1,142 (42%) tissue specific (TS)
165 lncRNAs (**Fig. 2b, Supplementary Table 5**). To assess how well TS lncRNAs distinguish cancers, we
166 performed clustering based on the top five highest expressed TS lncRNAs per cancer (30 total). The
167 expression of just these lncRNAs was sufficient to cluster samples of the same cancer type (**Fig. 2c**).
168 Furthermore, the blood and solid cancers separately clustered together with little expression overlap
169 observed between the two groups across the 30 genes (**Fig. 2c**). Finally, we identified a similar proportion
170 of TS lncRNAs (38%, n = 1624) across 12 adult cancers from The Cancer Genome Atlas (TCGA) (**Online**
171 **Methods**) and observed that adult cancer tissue types were also well distinguished based on the
172 expression of the top 5 most TS lncRNAs (**Supplementary Fig. 2f-g**).
173 Notably, NBL tumors expressed 2.5x more TS lncRNAs (n=522) than the cancer with the next
174 highest: WT (TS lncRNAs: n=211), and 10x more than AML, which had the least number of TS lncRNAs
175 (n=49) (**Fig. 2b**). To validate NBL's striking quantity of TS lncRNAs, we first assessed whether immune
176 and stromal cell infiltration[36] could be contributing to the variety of lncRNAs expressed. We ran the

177 ESTIMATE algorithm as previously described[36] (**Online Methods**) to determine levels of immune and
178 stromal cell presence in each tumor sample using expression data. Using these purity estimates, we re-
179 calculated each cancer's tau score and restricted our analysis to NBL samples with either 80% or 90%
180 purity. In both cases, we found that NBL still had the greatest number of TS lncRNAs (n =588 – NBL 90%
181 purity) compared to other cancers (**Supplementary Table 6**). Finally, given that the TARGET NBL RNA-
182 seq dataset is un-stranded, we validated our findings using stranded RNA-seq data in an independent
183 NBL cohort generated through the Gabriela Miller Kids First (GMKF) program (n=223). We observed that
184 48% of expressed lncRNAs were tissue specific in the GMKF cohort, an increase from the 31% observed
185 in the TARGET cohort (**Supplementary Table 6**). These results confirm lncRNA abundance in NBL and
186 demonstrate that the tau score robustly identifies TS lncRNAs across varying datasets.
187

188 **Somatic DNA copy number alterations impact lncRNA expression**

189 Many pediatric cancers are marked by a lower single nucleotide variant (SNV) and insertion-deletion
190 (indel) burden than observed in adult cancers[36]. Instead, large chromosomal events, such as somatic
191 copy number aberrations (SCNAs) and other structural variants (SVs) have been shown to dysregulate
192 protein coding driver genes[36,44]. However, the extent to which large chromosomal alterations impact
193 lncRNAs in pediatric cancers remains unknown. We thus sought to identify SCNAs and SVs using
194 whole genome sequencing (WGS) data from the TARGET project available for NBL (n=146), B-ALL
195 (n=302), AML (n=297), and WT (n=81) (**Online Methods**). We observed that NBL had the greatest
196 frequency of copy number events (**Supplementary Fig. 3a**). The GISTIC v2 algorithm[45] was applied
197 to detect regions of recurrent SCNA (q-value < 0.25). We identified 673 expressed lncRNAs
198 overlapping 176 significant SCNA regions across the cancers (**Supplementary Table 7**). WGS
199 samples with matched RNA-sequencing were then used to compare lncRNA expression in samples
200 with or without an SCNA event and determine significant differential expression (DE) (**Online**
201 **Methods**, **Supplementary Table 8**). Across all cancers, between 10-30% of expressed genes
202 overlapping SCNA regions showed significant differential expression based on SCNA, a proportion

203 that was similar for both PCGs and lncRNAs (**Fig 3a**). Altogether, there were 198 (29%) unique
204 lncRNAs with significant DE due to SCNA (**Supplementary Fig 3b**). The majority of the significantly
205 dysregulated lncRNAs were identified in the two cancers with the greatest overall number of
206 expressed lncRNAs, NBL and WT, and mapped to regions with highly recurrent SCNAs in those
207 cancers (chromosomes 1, 7, 11, and 17) (**Fig 3b**).

208 While SCNAs can cause the dysregulation of lncRNA expression based on gene dosage,
209 structural variant (SV) breakpoints within a lncRNA could cause loss or gain of function[36,44]. We utilized
210 WGS data to identify lncRNAs disrupted by SV breakpoints using a previously described combination
211 approach involving copy number read-depth and discordant junction approach[44] (**Online Methods**).
212 There were 650 unique expressed lncRNA genes disrupted by SVs, 89% of which were found in only
213 one sample (**Supplementary Fig. 4a)**. We observed 212 SV-impacted lncRNA genes located at
214 SCNA regions (**Fig. 3c**), and 65% of lncRNAs genes disrupted by SV breakpoints in at least five
215 samples were located at SCNA regions (**Supplementary Fig. 4b, Supplementary Table 9**). Indeed,
216 the top-ranked SV-impacted lncRNA in both NBL and WT, *MYCNOS,* associates with the disease-
217 driving chr2p24 amplification[46,47] (**Supplementary Fig. 4c-d)**. In B-ALL, the SV-impacted lncRNAs:
218 *KIAA0125* and *CDKN2B-AS1 (ANRIL)* associate with the well-studied *IGH* translocation and
219 *CDKN2A*/*B* deletion locus (**Supplementary Fig. 4e**)[48]. The top-ranked SV-impacted lncRNA in AML,
220 *MIR181A1HG (MONC)*, associates with a recurrent SCNA deletion on 1q and is mildly up-regulated
221 in the AML dataset (p = 0.061, **Supplementary Fig. 4f**). *MIR181A1HG* (*MONC*) was described
222 previously as an oncogene in acute megakaryoblastic leukemia[49,50]. Finally, we observed 30 lncRNAs
223 with pan-cancer (n>3) expression and SV breakpoints(**Supplementary Fig. 4h**). The most number of
224 breakpoints across unique samples was observed in *LINC00910,* which was shown previously to be
225 essential for cell growth in the K562 cell line[51].

226

227 **Characterization of transcriptional network perturbation mediated by dysregulated lncRNAs**

228 To determine how lncRNAs may drive pediatric cancers, we examined the downstream impact of
229 lncRNAs on gene regulation. We focused on identifying lncRNAs that mediate transcriptional regulation
230 by modulating TF activity (lncRNA modulators)[52-55]. We wrote custom scripts implementing the lncMod
231 computational framework[56] (**Online Methods**) to first identify DE-lncRNAs and then to assess their
232 impact on correlated expression between a TF and its target genes[21,56] (**Fig. 4a, Online Methods**).
233 Across all cancers studied, we identified 313,370 unique, dysregulated lncMod triplets (lncRNA-TF-target
234 gene), representing 0.02-0.2% of possible triplets, which have significant correlation differences between
235 a TF and target gene upon lncRNA expression dysregulation (**Supplementary Table 10-11**). This
236 proportion was consistent with previous findings from the lncMap study in adult cancers[21], although more
237 triplets were identified in datasets with greater sample size (**Supplementary Table 10-11**). LncRNA
238 modulators were categorized into one of three categories based on their impact on TF-target gene
239 correlation; either the correlation was enhanced, attenuated, or inverted (**Fig 4a-b**). lncRNA modulators
240 have context specific function such that for different TF-target gene pairs they could exert different types
241 of regulation (**Supplementary Fig. 5b**). The majority of lncRNA modulators appeared to be active in only
242 one cancer, with only 15% (138 of 923 lncRNAs) having pan-cancer activity (n>3) (**Fig. 4c**).

243 To determine the biological impact of lncRNA modulators, we identified lncRNAs whose target
244 genes were enriched in MSigDB's Hallmark Gene Sets (HMS)[57] (Fisher's exact test, FDR < 0.1; **Online**
245 **Methods**). Across the majority of cancers, lncRNA modulator target genes had significant enrichment in
246 the proliferation, metabolism, and DNA damage hallmark categories (FDR range: 0.1 to $2.24 \times 10^{-36}$; **Fig.**
247 **4d**). Overall, the top-enriched hallmark pathways closely mirrored those found for lncRNA modulators in
248 adult cancers[22]. Consistent with its role in development and as an oncogene in certain cancers [23], the
249 top-enriched hallmarks for the *H19* lncRNA, dysregulated in NBL, were the EMT (development) and G2M-
250 checkpoint (proliferation) hallmarks (**Supplementary Fig. 5c**). The blood cancers exhibited strong
251 enrichment of lncRNA modulators regulating MYC targets, which has a well-established role in
252 leukemias[58]. Furthermore, in AML, we observed that gene targets of the myeloid-specific lncRNA,

253 *HOTAIRM1*, were most enriched for proliferation hallmarks (**Supplementary Fig. 5d**), consistent with
254 this lncRNA's known role in proliferation as an oncogene in adult AML[59].

255 Finally, we sought to determine potential lncRNA mechanism by identifying recurring patterns of
256 regulation amongst lncMod triplets. To this end, we nominated candidate lncRNA-TF associations by
257 ranking TF's based on the number of target genes regulated by each given TF (**Supplementary Table**
258 **12**). As proof-of-concept, we were able to detect known lncRNA-TF associations such as *GAS5* with
259 E2F4[60] (RNA-protein), and *SNHG1* with *TP53*[61] (RNA-RNA) amongst lncMod triplets in our study
260 (**Supplementary Fig. 5e-f**). A notable example from the hundreds of novel associations identified is
261 between the B-ALL specific lncRNA, *BLACE* (B-cell acute lymphoblastic leukemia expressed, tau score:
262 0.999) and its top associated TF, XBP1, which has known roles in pre-B-ALL cell proliferation and
263 tumorigenesis[62] (**Fig 4e-f)**. These predictions of lncRNA transcriptional networks provide focused
264 avenues to elucidate the mechanisms through which lncRNAs can drive pediatric cancers.

265

266 **Defining the role of lncRNAs in childhood cancer development**

267 Pediatric cancers arise in the context of normal human development where cells do not differentiate as
268 they should, resulting in malignant cell transformation[63]. Some tumors are comprised of heterogenous
269 cells that resemble varying differentiation lineages with distinct transcriptomic states due to distinct super
270 enhancer transcription factor networks[64,65]. We sought to uncover lncRNAs associated with these varying
271 cell lineages as they may contribute to pediatric cancer etiology. We used NBL as a model given its
272 heterogeneity and two confirmed tumor cell states: the undifferentiated mesenchymal (MES) cells and
273 the committed adrenergic (ADRN) cells, which can interconvert[66]. Given that NBL precursor cells, the
274 neural crest cells, have been shown to have a more MES gene expression signature[65,66], we
275 hypothesized that lncRNAs correlated with an MES signature may play a role in NBL development. Using
276 the gene set variation analysis (GSVA) method[67] we assigned for each NBL Stage 4 sample, both a MES
277 and ADRN score (**Online Methods**). Using hierarchical clustering (**Supplementary Figure 6a**) we

278 categorized samples based on their primary gene expression phenotype as ADRN, MES, or mixed (**Fig**
279 **5a**). We next correlated the MES and ADRN score with lncRNA expression across NBL samples. We
280 observed 29 lncRNAs associated with MES samples and 21 lncRNAs associated with ADRN samples
281 (**Fig 5b**) (Spearman's |rho| >0.6, adj. pval < 0.01). We then performed a guilt-by-association analysis[68]
282 to determine the potential functional pathway for these lncRNAs based on the pathway of their correlated
283 protein coding genes (**Online Methods**). Gene set enrichment was performed using the gene ontology
284 (GO) biological processes gene set. Intriguingly, the ADRN group of lncRNAs showed enrichment for
285 DNA replication and cell cycle associated gene sets, whereas the MES lncRNAs were associated with
286 organ development and immune response (**Fig 5b**). We validated these same pathway results in an
287 independent analysis of the GMKF NBL cohort restricted to Stage 4 samples (n=67) (**Supplementary**
288 **Figure 6b**). Across both TARGET and GMKF cohorts we observed 13 lncRNAs strongly associated with
289 MES samples (**Supplementary Table 6c**), which warrant further study for their potential role in NBL
290 development.
291

292 **Identification of potential cancer driver lncRNAs via integration of epigenetic data**

293 To better identify ADRN lncRNAs we elucidated lncRNAs directly regulated by the known ADRN
294 transcription factors (TFs): MYCN, PHOX2B, HAND2, GATA3, ISL1, and TBX2[65,69]. This set of TFs, which
295 are co-bound and auto-regulated, are known as the core transcriptional circuitries (CRC) and drive the
296 ADRN cell lineage in NBL[65,69]. CRC gene regulation occurs both by direct promoter binding (**Fig. 5c-1**)
297 and by distal binding to either promoters (**Fig. 5c-2**) or enhancer regions (**Fig. 5c-3**) which then regulate
298 the gene of interest via long-range chromatin interactions[65,69-71]. CRC-bound regulatory loci were
299 identified from publicly available ChIP-seq data for all ADRN TFs across two MYCN-amplified NBL cell
300 lines: SKNBE(2)C and KELLY[69,72] (**Online Methods**). To comprehensively identify both short- and long-
301 range CRC gene regulation, we generated high-resolution (i.e. using 4-cutter restriction enzyme DpnII)
302 genome-wide promoter-focused Capture C[73] in the NBL cell line NB1643. After pinpointing gene

303 promoters interacting with CRC TF bound regulatory loci (promoters or enhancers) (**Fig. 5c, Online**
304 **Methods**), we identified 547 lncRNA genes associated with the NBL CRC (**Fig 5d, Supplementary**
305 **Table 13**), with only 249 of these lncRNA genes being bound by CRC TFs within their promoter regions.
306 We further distinguished 313 ADRN lncRNAs based on differential expression (DE) between ADRN and
307 MES samples (**Fig 5d, Supplementary Table 14**). The *TBX2-AS1* DE-lncRNA was highly correlated to
308 the CRC TF: *TBX2* (Pearson's r=0.77), and both are up-regulated in ADRN samples (**Fig 5e**). CRC
309 binding is observed at both the shared promoter region of *TBX2* and *TBX2-AS1* and at an interacting
310 distal enhancer (**Fig 5f**). TBX2 was recently shown to be involved in NBL cell proliferation,[74] but the role
311 of *TBX2-AS1* in NBL is unknown.

312 To further demonstrate the utility of this epigenetic based prioritization, we applied the same
313 method to T-ALL, which also has a well-established set of CRC TFs (TAL1, MYB, GATA3, and RUNX1)[71].
314 We used available ChIP-seq and ChIA-PET data for the TAL1 mutated T-ALL cell lines, Jurkat and
315 CCRF-CEM, to identify loci bound by the T-ALL CRC TF's[71] (**Online Methods**). We not only identified
316 the known leukemia associated lncRNA PVT1, but also 9 other T-ALL CRC lncRNAs prioritized based
317 on correlation with T-ALL PCGs and differential expression associated with a previously defined TAL1-
318 subgroup[75] (**Supplementary Figure 7, Supplementary Table 13-15**). Taken together, this novel data
319 integration method nominates multiple lncRNAs with previously unknown function for further study as
320 potential driver genes in pediatric cancer.

321

322 **Integrative multi-omic analysis prioritizes *TBX2-AS1* as a candidate functional lncRNA in NBL**

323 To obtain a comprehensive prioritization of candidate functional lncRNAs for each cancer histotype,
324 we integrated information for (1) tissue specific expression, (2) dysregulation due to DNA copy number
325 aberration, and (3) regulation by CRC TFs (**Supplementary Table 16**). Here, we focus on the NBL
326 cohort since this cancer has data available for all of the prioritization steps (**Supplementary Table**
327 **17**). The top ranked lncRNA in NBL was *MEG3*, which has a known role in both NBL and other

328 cancers[43]. The next notable lncRNA, *TBX2-AS1,* is up-regulated due to chromosome 17q gain (**Fig**
329 **6a**), has NBL-specific expression (tau score: *TBX2*- 0.807, *TBX2-AS1*- 0.86; **Supplementary Fig. 8a**),
330 and is co-regulated with *TBX2*. TBX2 has been shown to drive NBL proliferation via the *FOXM1*/*E2F1*
331 gene regulatory network[72] and we hypothesized that *TBX2-AS1* may play a similar role because
332 predictions from our lncMod analysis indicated that *TBX2-AS1* impacts E2F targets and G2M
333 checkpoint genes (**Fig. 6b**). Furthermore, the TFs primarily impacted by TBX2 knockdown[72], MYBL2
334 and E2F1, were found to have the most target genes predicted to be regulated by *TBX2-AS1* (**Fig 6c-**
335 **d**). Evidence for this association was further supported by the correlation (Spearman's rho > 0.4)
336 between *TBX2-AS1* and *TBX2*'s target TFs, including: *FOXM1*, *E2F1*, and *MYBL2* (**Supplementary**
337 **Fig. 8b**). While the strong correlation between *TBX2-AS1* and *TBX2* may confound our predictions, a
338 previous study showed positionally conserved lncRNAs[59], such as *TBX2-AS1*, often regulate their
339 neighboring developmental TFs (TBX2) and can play roles in genome organization and cancer[59].
340 Based on the promising *in silico* evidence, we prioritized *TBX2-AS1* for experimental study.

341
342 **Silencing of *TBX2-AS1* inhibits cell growth of neuroblastoma cells**

343 We assessed the role of *TBX2-AS1* using human-derived NBL cell line models. First, we evaluated
344 *TBX2-AS1* expression across 38 NBL cell lines using RNA-seq[76] (**Supplementary Fig 8c**). Expression
345 of *TBX2* and *TBX2-AS1* were subsequently validated in eight cell lines using RT-qPCR
346 (**Supplementary Fig. 8d**). We selected NLF and SKNSH models for further study based on their high
347 *TBX2-AS1* expression and differing expression levels of *TBX2*. Silencing of *TBX2-AS1* using small
348 interfering RNA (siRNA) achieved 92% and 63% reduction of *TBX2-AS1* expression in NLF and
349 SKNSH, respectively (**Fig. 6e**). We also observed down-regulation of TBX2 protein levels in the
350 siTBX2-AS1 treated cells for both cell lines (**Fig. 6f**). Given the known role of TBX2 in NBL cell
351 proliferation[74], we measured cell growth of siTBX2-AS1 treated NBL cells to determine if *TBX2-AS1*
352 has similar function. When the non-targeting control (siNTC) treated cells reached confluence, the
353 siTBX2-AS1 treated cell index was reduced by 42.6% and 36.8% (n=3, $p < 0.01$) in the NLF and

354 SKNSH cell line, respectively (**Fig. 6g-h, Supplementary Fig. 8e**). Live cell imaging using the
355 IncuCyte revealed changes in cell morphology for siTBX2-AS1 treated NLF cells, featuring an
356 appearance of disrupted cell to cell adhesion and elongated cell body (**Supplementary Fig. 8f**). To
357 identify pathways impacted by *TBX2-AS1* knockdown, we performed total RNA sequencing in triplicate
358 of NLF cells and compared gene expression in control (siNTC) vs siTBX2-AS1 treated cells
359 (**Supplementary Fig. 8g**). Gene set enrichment analysis (GSEA) of the 364 significantly up-regulated
360 genes (log-fold change > 1.5, adj pval < 0.1) revealed enrichment (FDR < 0.1) for hallmarks associated
361 with inflammation including: TNFA signaling and interferon gamma response (**Supplementary Table**
362 **18**). Across the 544 down-regulated genes, E2F target genes hallmark was most enriched. To
363 determine whether differentially expressed genes shared common regulation, we used the iRegulon
364 program[77], to search for TF motifs and ENCODE ChIP-seq tracks upstream of genes (**Online**
365 **Methods**). Using a normalized enrichment score (NES) of at least 3, we observed motif enrichment
366 for the neuronal differentiation repressor REST and the RFX family of transcription factors in 59% of
367 siTBX2-AS1 up-regulated genes (**Fig. 6i**). In 42% of downregulated genes, the top enriched TFs were
368 MYBL2 and E2F1, corroborating our GSEA results. Moreover, both the growth assays and gene
369 expression profiling confirmed our lncMod results, which showed that *TBX2-AS1* impacts NBL
370 proliferation by modulating target genes of E2F1 and MYBL2 (**Fig. 6b-d**). These data thus demonstrate
371 the utility of our integrative lncRNA characterization and prioritization approach for future validation
372 experiments across all cancers considered in this study. Furthermore, we uncovered a functional role for
373 *TBX2-AS1* in NBL proliferation likely mediated via the regulation of TBX2 and its known target genes:
374 E2F, MYBL2, and REST[72].

375

376 **Discussion**

377 LncRNAs have emerged as important regulators of gene expression and their dysregulation can impact
378 key cancer pathways and drive tumorigenesis[1-4]. Despite this, relatively few lncRNAs have been

379 experimentally characterized and the landscape of lncRNA expression across pediatric cancers has been
380 previously unknown. In this study, we explored lncRNA expression, cancer association, and regulatory
381 networks across 1,044 pediatric leukemias and solid tumors, representing six different cancer types. The
382 breadth of samples and cancer types included allowed for robust identification of novel, cancer-specific,
383 and developmental lncRNAs. Furthermore, we used systems modelling to identify expression patterns
384 for both up- and downstream lncRNA gene regulation. Altogether we provide multi-dimensional insight
385 into the predicted biological and functional relevance of lncRNAs by integrating WGS, ChIP-seq,
386 chromatin capture, and predictions of transcriptional networks.
387
388 Analysis of the lncRNA landscape across pediatric cancers revealed the histotype and context-
389 specific nature of lncRNAs. We report a total of 2,657 robustly expressed lncRNAs across the six cancer
390 types studied. This number is notably smaller than reports from pan-cancer studies of adult
391 malignancies[15,17], likely due to the smaller number of cancer types studied here and conservative
392 expression threshold applied. However, similar to our findings in adult cancers, 43% (1,142/ 2,657) of
393 expressed lncRNAs exhibited tissue-specific (TS) expression across pediatric cancers. Indeed, lncRNAs
394 had significantly greater tissue specificity than protein coding genes, making them more ideal candidates
395 as biomarkers. Currently there is one lncRNA, *PCA3*, that is FDA-approved as a biomarker for prostate
396 cancer[78] and multiple trials investigating ncRNAs in cancer prognostics are underway[79]. In this study, the
397 top five most TS lncRNAs per cancer were sufficient to differentiate each cancer histotype. Furthermore,
398 we identify lncRNAs specific to distinct cell lineages within NBL, suggesting there is potential for lncRNAs
399 to be used as highly sensitive markers to differentiate cancer subtypes more accurately.
400
401 Typically, investigation of lncRNA dysregulation involves comparing lncRNA expression between
402 cancer and normal control samples and is an analysis that amply yields adult-cancer associated
403 lncRNAs[15]. However, the lack of normal expression controls for the majority of pediatric cancers[36] is a
404 major complication in defining pediatric cancer-associated lncRNAs. To overcome this, we leveraged

405 information about how pediatric cancers are epigenetically regulated. In particular, NBL, is composed of
406 two cells lineages representing different development stages and each with distinct super-enhancer
407 transcription factor networks. Given the tie between organogenesis and tumorigenesis in pediatric
408 cancer[63], we hypothesized that lncRNAs associated with these cell states may also be involved in NBL
409 development. After correlation and pathway analysis, we discovered that lncRNAs associated with the
410 mesenchymal cell lineage had enrichment for organogenesis gene sets, while adrenergic-associated
411 lncRNAs were predicted to be involved in proliferation based on enrichment for DNA replication and cell
412 cycle gene sets. The majority of NBL samples have cells with an adrenergic gene expression signature,
413 which could suggest that ADRN lncRNAs are major drivers of disease and thus potential therapeutic
414 targets. To better identify these ADRN lncRNAs, we integrated ChIP-sequencing of core regulatory
415 (CRC) transcription factors for ADRN cells with our expression data to identify cancer driver lncRNAs.
416 CRC TFs bind to cell-type-specific enhancers and regulate the expression of cell-type-specific genes[80].
417 By taking advantage of this information we were able to prioritize lncRNAs likely to be important for cancer
418 cell identity based on CRC TF regulation. CRC TFs have been well defined for NBL and T-ALL[69,71];
419 however the fact that they largely bind enhancer regions necessitated that we also use chromatin
420 interaction data to accurately determine regulated genes. Incorporation of these datasets allowed us to
421 identify 2-fold more CRC regulated lncRNAs in NBL and 3-fold in T-ALL as compared to using just ChIP-
422 seq data alone, which restricts lncRNA identification to those with CRC TFs bound at their promoter.
423 Notably, there were ten common CRC-regulated lncRNAs between NBL and T-ALL, and an important
424 next step for further identification of pan-pediatric cancer associated lncRNAs is application of this novel
425 analysis to a broader set of pediatric cancers.
426
427 While upstream regulation can help nominate cancer-associated lncRNAs, determining the
428 mechanism through which dysregulated lncRNAs impact downstream target genes is also crucial.
429 However, prediction of lncRNA function is limited given that very few lncRNA mechanisms have been
430 fully established and lncRNAs lack conserved sequence and structure[81]. Many studies instead use

431 correlated protein coding gene expression as a proxy to define lncRNA pathways, but this approach often
432 results in many false positives and does not provide mechanistic insight[81]. To address this, we used the
433 lncMod method[21,56] to model the functional mechanism of dysregulated lncRNAs by examining correlated
434 changes in transcription factor to target gene regulation. We used motif presence and regression analysis
435 to identify TF-target gene relationships, though future studies will be strengthened by incorporating TF
436 ChIP-seq data, when it becomes more widely available for pediatric cancers. Nevertheless, we were able
437 to successfully associate lncRNAs to TFs with known interactions, such as SNHG1 with TP53, while also
438 providing a prioritized list of novel associations that serve as a starting point for future experimental
439 studies such as RIP/MS[82] and ChiRP-seq[83]. Finally, while our lncMod analysis was focused on
440 transcriptional regulation, the addition of microRNA binding and RNA-binding protein data, as utilized in
441 adult cancers[22], is an important next step in understanding how lncRNAs impact post-transcriptional
442 regulation in pediatric cancers.
443
444 Our study delineated high confidence lncRNA expression across pediatric cancers within the
445 restrictions set by the sequencing depth and RNA-seq type available per cancer dataset. We required
446 RNA-seq samples included in our study to have at least 10 million reads and read length of at least 75
447 bp; and with the exception of the T-ALL samples, all samples were poly-A selected. Future studies
448 involving total RNA-seq, greater sequencing depth, and longer read sizes could capture a larger diversity
449 and more accurate set of expressed lncRNAs by accounting for non-polyadenylated genes and
450 identifying scarcer or temporally expressed lncRNAs. Nevertheless, our high confidence set of lncRNAs
451 are very likely to be functional given that low or rare expression can be an indicator of transcriptional
452 noise[84]. In addition to having a limited number of RNA matched WGS samples, the Complete Genomics
453 short read technology limits the detection of structural variants based on size as previously described[36,44].
454 The use of long-read sequencing and greater sequencing depth in future studies will enable more
455 accurate copy number and structure variant detection in pediatric cancers.
456

457 Finally, multi-dimensional integration of our computational predictions resulted in the nomination
458 of functionally relevant lncRNAs in each pediatric cancer. We annotated tissue specificity, copy number,
459 pathway, and likely targets for these lncRNAs, providing a solid foundation for mechanistic studies. As
460 proof-of-principle, we demonstrate that the top-prioritized tissue-specific and copy number dysregulated
461 lncRNA, *TBX2-AS1,* impacts NBL cell growth, validating our approach, while transcriptomic profiling
462 corroborated our pathway predictions. Knockdown of *TBX2-AS1*, showed downregulation of genes
463 regulated by E2F1 and MYBL2, the same TFs impacted upon TBX2 knockdown[72]. Future studies could
464 reveal whether *TBX2-AS1* modulates TBX2 through direct binding or by impacting transcriptional
465 regulation at their shared locus. *TBX2-AS1* was previously shown to be among a group of lncRNAs which
466 are positionally conserved and near developmental associated TFs[59]. This group of lncRNAs and their
467 neighboring TFs, typically have tissue specific expression, can be involved in cancer development, and
468 affect each other's expression[59], all of which we observed for TBX2 and *TBX2-AS1*. Together these
469 genes contribute to the proliferative state of NBL cells and could have potential as novel therapeutic
470 targets.

471 Altogether, this study provides a comprehensive characterization of lncRNAs across pediatric
472 cancers and serves as a rich resource for future mechanistic studies; these data may aid in the selection
473 of cancer biomarkers and candidate therapeutic lncRNA targets.

474

475

476

477

478

479

480 **Online Methods**
481

482 **RNA-seq data processing.** A comprehensive RNA-seq analysis pipeline was used on all samples
483 (Supplementary Table 1, Supplementary Fig 1). First FASTQC was run on all samples and any samples
484 that had a Phred score < 30 for more than 25% of read bases were removed. Samples were then aligned
485 using STAR_2.4.2a [85] with the following parameters: "STAR --runMode alignReads --runThreadN 10 --
486 twopassMode Basic --twopass1readsN -1 --chimSegmentMin 15 --chimOutType WithinBAM –genomeDir
487 X--genomeFastaFiles ucsc.hg19.fa --readFilesIn fasta1 fasta2 --readFilesCommand zcat --outSAMtype
488 BAM SortedByCoordinate --outFileNamePrefix X --outSAMstrandField intronMotif --quantMode
489 TranscriptomeSAM GeneCounts --sjdbGTFfile gencode.v19.annotation.gtf --sjdbOverhang X." To
490 assess the quality of the aligned RNA-seq data we ran MultiQC [86], and removed samples with < 70%
491 uniquely mapped reads and < 10 million mapped reads.
492

493 **Gene/transcript mapping and quantification.** To map reads to genes and quantify gene expression
494 we ran StringTie 1.3.3 [37]. StringTie involves three steps, first quantifying expression of both known and
495 novel gene transcripts using an annotation guided approach. We used the Gencode v19 gene annotation
496 to guide gene detection.1) "stringtie bamfile -G gencode.v19.annotation_stringtie.gtf -B --rf -o out.gtf -A
497 gene_abund.tab -C cov_refs.gtf -p 10. " In the second step, StringTie merges the gene annotation across
498 all samples such that there is a uniform annotation for known and novel gene transcripts in one
499 transcriptome gtf file. 2) "stringtie All_PanTARGET_PreMerge_StringTie_Files.txt --merge -G
500 gencode.v19.annotation_stringtie.gtf -o StringTie_PanCancer_AllMergedTranscripts.gtf." Finally,
501 StringTie is run again to quantify expression using the PanTarget transcriptome gtf file and de novo gene
502 transcript detection is turned off. 3) "stringtie bamfile -G StringTie_PanCancer_AllMergedTranscripts.gtf
503 -B -e --rf -o out.gtf -A gene_abund.tab -C cov_refs.gtf -p 10"
504

505 **Comparison of pan-TARGET transcriptome with reference annotation.** Novel transcripts were
506 assigned as an isoform of a known gene based on exonic overlap (>50% by bp) with genes in either the
507 GENCODE v19 or RefSeq v74 databases using custom Python scripts. Any remaining novel transcripts
508 were assigned as novel genes (MSTRG_Merged.# or MSTRG.#) based on overlapping exon positions.
509 Novel genes were further filtered based on read coverage, in that we required that at least one transcript
510 for a novel gene have more than one exon with at least 5 reads in at least 20% of samples per cancer.
511 High confidence novel genes were required to have at least 3 exons. Finally, for all transcripts (known
512 and novel), to obtain gene level quantification, transcript FPKM and count values were summed to get a
513 gene level value.
514
515 **Prediction of novel gene coding potential and lncRNA gene annotation.** We predicted coding
516 potential of novel transcripts using the PLEK v1 algorithm tool [39]. PLEK uses a support vector machine
517 (SVM) for a binary classification model to distinguish a lncRNA versus a coding mRNA. The features
518 used as input for the SVM are calibrated k-mer usage frequencies of a transcript's sequence. PLEK has
519 previously been validated on RefSeq mRNAs and GENCODE lncRNAs (the main reference annotations
520 used in our study) and has achieved >90% accuracy in predicting gene coding potential [39]. To further
521 delineate lncRNAs, we removed any predicted novel non-coding transcripts that were < 200bp (sum of
522 total exon length). We updated the gene type of GENCODE v19 genes with the gene type of genes that
523 had matching gene names in GENCODE v29. Additionally we filtered out lncRNA genes that have been
524 deprecated in Gencode v29. Finally, some lncRNA genes in Gencode v19, have both a lncRNA and small
525 RNA transcript. For these 147 cases we did not include the small RNA transcript when summing gene
526 transcripts to obtain gene level expression.
527
528 **Tissue specific gene expression.** The tau score, a measure of the tissue specific expression of a gene
529 was calculated as described by Yanai et. al[41]. The formula for the score is listed below. $x_i$ is defined as

530 the mean expression of a gene in a particular cancer and n is the total number of cancers considered, in
531 this case n = 6.

$$\tau = \frac{\sum_{i=1}^{n}(1-\hat{x_i})}{n-1}; \hat{x_i} = \frac{x_i}{\max\limits_{1\leq x\leq n}(x_i)}$$

532

533 **CNV detection, processing, and impact on gene expression.** Copy number calls were made by
534 Complete Genomics (CGI) from WGS for NBL, WT, AML, and B-ALL. We used CGI
535 files"somaticCnvDetailsDiploidBeta" containing ploidy estimates and tumor/blood coverage along 2kb
536 bins across the genome. To create segmentation files, we used custom scripts to reformat CGI coverage
537 data to meet requirements of the "copynumber" R bioconductor package as previously described[44]. We
538 used the winsorize function in this package, which performs data smoothing and segmentation via a
539 piecewise constant segmentation (pcf) algorithm (kmin =2 and gamma= 1000). Segmentation files were
540 visualized using the R package svpluscnv (https://github.com/ccbiolab/svpluscnv)
541 https://doi.org/10.1093/bioinformatics/btaa878. We then ran GISTIC2.0, using segmentation data as
542 inputs and parameters: "GISTIC2 -v 30 -refgene hg19 -genegistic 1 -smallmem 1 -broad 1 -twoside 1 -
543 brlen 0.98 -conf 0.90 -armpeel 1 -savegene 1 -gcm extreme -js 2 -rx 0". To determine which genes copy
544 number impacts, we intersected CNV regions listed in the "all_lesions.conf_90.txt" file from GISTIC output
545 with gene positions. We used section 1 from the "all_lesions.conf_90.txt" file to assign a binary descriptor
546 to each gene as either being not amplified or deleted (CNV-no) if the sample had actual copy gain 0 for
547 the region containing the gene. We assigned CNV-yes if the region containing the gene was amplified or
548 deleted, which included samples with actual copy gain 1 or 2, where 1 indicates low level copy number
549 aberration (exceeds low threshold of copy number: 1: 0.1<t< 0.9) and 2 indicates a high level of copy
550 number aberration, CNV exceeds high threshold (t>0.9) according to GISTIC. To determine CNV impact
551 on gene expression, we assessed differential expression of the gene in samples from the two groups
552 (CNV yes or no) using Wilcoxon rank sum test ($p < 0.01$). Genes were considered to have evidence of

553 differential expression due to copy number if the absolute value of the log2 fold change between the two
554 groups was > 0.58 and $p < 0.05$.
555
556 **Structural variant detection and filtering.** Structural variants were identified from WGS as previously
557 described[44]. Somatic sequence junctions that were completely absent in the normal genome are reported
558 by Complete Genomics (CGI) in the somaticAllJunctionsBeta file. To obtain a high confidence set of
559 junctions, where there is a likely true physical connection between the left and right sections of a junction,
560 the following filtering was applied by CGI to obtain the highConfidenceSomaticAllJunctionsBeta.
561
562 1) DiscordantMatePairAlignments ≥ 10 (10 or more discordant mate pairs in cluster
563 2) JunctionSequenceResolve = Y (local de novo assembly is successful)
564 3) Exclude interchromosomal junction if present in any genomes in baseline samples
565 (FrequencyInBaseline > 0)
566 4) Exclude the junction if overlap with known underrepresented repeats
567 (KnownUnderrepresentedRepeat = Y): ALR/Alpha, GAATGn, HSATII, LSU_rRNA_Hsa, and
568 RSU_rRNA_Hsa
569 5) Exclude the junction if the length of either of the side sections is less than 70 base pairs.
570
571 Further filtering of these high confidence structural variants included removing rare/common germline
572 variants that passed the CGI filters. We used the Database of Genomic Variants (DGV v. 2016-05-15,
573 GRCh37) in order to remove SVs that had at least 50% reciprocal overlap with DGV annotated common
574 events and were type matched.
575
576 **Structural variant analysis.** To obtain a comprehensive landscape of SVs we combined both the
577 sequence junction and copy number read depth approaches to identify SVs, with co-localizing break
578 points being orthogonally validated. Recurrence of SVs was considered based on overlap with genes
579 from our pan-pediatric cancer transcriptome. Genomic overlap between SVs and genes was determined
580 using the bedtools intersect tool (default parameters). Variants were assigned to genes based on if the

581 sequence junction (left/right position) + 100 bp overlapped gene coordinates +/- 2.5kb. Genes were then
582 ranked based on the number of unique samples per cancer with a SV breakpoint.
583
584 **Gene signature analysis.** We obtained a list of genes associated with the mesenchymal (MES) and
585 adrenergic (ADRN) NBL cell types from GEO (GSE90805). We then used the GSVA R package[67] with
586 the Poisson kernel (kcdf) parameter to assign a score per sample representing the total expression
587 enrichment of genes associated with either the MES or ADRN cell types. We performed hierarchical
588 clustering to divide NBL samples into three groups (MES, ADRN or mixed phenotype) based on
589 expression of MES and ADRN genes using the pheatmap R package and cutting the dendrogram at n=3.
590 We correlated the MES and ADRN score with lncRNA expression across Stage 4 NBL TARGET cohort
591 and GMKF cohort samples separately and identified lncRNAs as having significant correlation based on
592 absolute value Spearman's rho > 0.6. These lncRNAs were then labeled as MES or ADRN based on
593 significant correlation with either the MES or ADRN score. We next repeated score correlation with PCGs.
594 We performed a guilt-by-association analysis assigning MES/ADRN PCGs and by association their
595 correlated MES/ADRN lncRNAs (Spearman rho > 0.5) to pathways using Fisher exact test, FDR < 0.1
596 for gene sets in the gene ontology (GO) biological processes collection.
597
598 **ChIP-seq data analysis.** To determine which lncRNAs are regulated by transcription factors involved in
599 the core regulatory circuitry (CRC) we utilized previously generated and analyzed histone and
600 transcription factor ChIP-sequencing data for NBL and T-ALL. For NBL, we used peak files for our
601 previously generated histone ChIP-seq data of: H3K27ac, H3K4me1, H3K4me3 for the BE(2)C cell line[87],
602 available on GEO: GSE138315. We downloaded raw sequencing files for CRC transcription factor ChIP-
603 seq data for MYCN, PHOX2B, HAND2, GATA3, TBX2, and ISL1 for the BE(2)C and KELLY cell lines
604 from GEO: GSE94822[69] and selected peaks with q-value < 0.001 for further analysis. We identified
605 regions in the genome where at least 4/6 of the transcription factors overlapped. This was obtained using
606 the homer mergePeaks tool: "mergePeaks -d 1000 -cobound 6 bed_file1… bed_file6" and the resulting

607 coBoundBy4 output file. For the T-ALL CRC we obtained overlapping CRC transcription factor loci for
608 TAL1, GATA3, and RUNX1 from the study by Sanda et. al[71], GEO: GSE29181 for both the Jurkat and
609 CCRF-CEM cell lines and integrated ChIP-seq data for the MYB transcription factor from GEO:
610 GSE59657[70], only available in the Jurkat line. We selected loci for further analysis if they were bound by
611 TAL1, GATA3, and RUNX1 as previously annotated by Sanda et. al.
612
613 **Identification of CRC transcription factor regulated genes.** To identify genes regulated by the NBL
614 or T-ALL CRC we considered CRC TF binding at both the gene's promoter and other regulatory region
615 interacting with the gene's promoter. We first overlapped CRC regions using bedtools intersect with gene
616 transcript promoter regions, which we defined as 3000bp upstream and downstream of the transcripts
617 first exon. For NBL, we then utilized the promoter-focused Capture C data, inclusive of all interactions
618 within 1Mb on the same chromosome, to identify genomic regions that were both bound by NBL CRC
619 TFs and interacting with a gene's promoter. To determine this, we used bedtools intersect to determine
620 overlap (minimum 1bp) between CRC bound loci with loci involved in chromatin interactions. From these
621 regions, we determined which interacting regions corresponded with a lncRNA promoter region. We
622 performed a similar analysis in T-ALL, however we utilized publicly available SMC1 (cohesin) ChIA-PET
623 data available on the ENCODE project to consider chromatin interactions.
624
625 **Promoter-focused Capture C data generation.** High resolution promoter-focused Capture C was
626 performed in the neuroblastoma cell line, NB1643, (untreated) in triplicate. Cell fixation, 3C library
627 generation, capture C, and sequencing was performed as described by Chesi et. al (2019) and Su et al
628 (2020). For each replicate, $10^7$ fixed cells were centrifuged to cell pellets and split to 6 tubes for a pre-
629 digestion incubation with 0.3%SDS, 1x NEB DpnII restriction buffer, and dH2O for 1hr at 37ºC shaking
630 at 1,000rpm. A 1.7% solution of Triton X-100 was added to each tube and shaking was continued for
631 another hour.10 ul of DpnII (NEB, 50 U/µL) was added to each sample tube and continued shaking for 2
632 days. 100uL Digestion reaction was then removed and set aside for digestion efficiency QC.The

633 remaining samples were heat inactivated incubated at 1000 rpm in a MultiTherm for 20 min, at 65°C to
634 inactivate the DpnII, and cooled on ice for 20 additional minutes. Digested samples were ligated with 8
635 uL of T4 DNA ligase (HC ThermoFisher, 30 U/µL) and 1X ligase buffer at 1,000 rpm overnight at 16°C
636 .The ligated samples were then de-crosslinked overnight at 65°C with Proteinase K (20 mg/mL, Denville
637 Scientific) along with pre-digestion and digestion control. Both controls and ligated samples were
638 incubated for 30 min at 37°C with RNase A (Millipore), followed by phenol/chloroform extraction, ethanol
639 precipitation at -20°C, then the 3C libraries were centrifuged at 3000 rpm for 45 min at 4°C to pellet the
640 samples. The pellets of 3C libraries and controls were resuspended in 300uL and 20µL dH2O,
641 respectively, and stored at −20°C. Sample concentrations were measured by Qubit. Digestion and
642 ligation efficiencies were assessed by gel electrophoresis on a 0.9% agarose gel and also by quantitative
643 PCR (SYBR green, Thermo Fisher).

644 Isolated DNA from 3C libraries was quantified using a Qubit fluorometer (Life technologies), and
645 10 µg of each library was sheared in dH2O using a QSonica Q800R to an average fragment size of
646 350bp.QSonica settings used were 60% amplitude, 30s on, 30s off, 2 min intervals, for a total of 5
647 intervals at 4 °C. After shearing, DNA was purified using AMPureXP beads (Agencourt). DNA size was
648 assessed on a Bioanalyzer 2100 using a DNA 1000 Chip (Agilent) and DNA concentration was checked
649 via Qubit. SureSelect XT library prep kits (Agilent) were used to repair DNA ends and for adaptor ligation
650 following the manufacturer protocol. Excess adaptors were removed using AMPureXP beads. Size and
651 concentration were checked again by Bioanalyzer 2100 using a DNA 1000 Chip and by Qubit fluorometer
652 before hybridization. One microgram of adaptor-ligated library was used as input for the SureSelect XT
653 capture kit using manufacturer protocol and custom-designed 41K promoter Capture-C probe set. The
654 quantity and quality of the captured libraries were assessed by Bioanalyzer using a high sensitivity DNA
655 Chip and by Qubit fluorometer. SureSelect XT libraries were then paired-end sequenced on Illumina
656 NovaSeq 6000 platform (51bp read length) at the Center for Spatial and Functional Genomics at CHOP.
657

658 **Promoter-focused Capture C data analysis.** Paired-end reads from each replicated were pre-
659 processed using the HICUP pipeline (v0.5.9), with bowtie2 as aligner and hg19 as the reference genome.
660 The unique ditags output from HiCUP were further processed by the chicagoTools bam2chicago.sh script
661 before significant promoter interaction calling. Significant promoter interactions at 1-DpnII fragment
662 resolution were called using CHiCAGO (v1.1.8) with default parameters except for binsize set to 2500.
663 Significant interactions at 4-DpnII fragment resolution were also called using CHiCAGO with artificial
664 baitmap and rmap files in which DpnII fragments were concatenated *in silico* into 4 consecutive fragments
665 using default parameters except for removeAdjacent set to False. Interactions with a CHiCAGO score >
666 5 in either 1-fragment or 4-fragment resolution were considered as significant interactions. The significant
667 interactions were finally converted to ibed format in which each line represents a physical interaction
668 between fragments.
669
670 **Differential gene expression analysis for T-ALL subtypes.** We identified differentially expressed
671 genes using the DESeq2 tool. We compared expression between the TAL1 subgroup and non-TAL1
672 subgroup, defined by Liu, et al[75]. We ran DESeq2 using default parameters and considered genes as
673 significantly differentially expressed if their absolute value of the log2 fold change was > 0.58 and their
674 Benjamini-Hoschberg adjusted-p value was < 0.01.
675
676 **lncMod implementation: transcription factor target gene regulation.** We developed custom Python
677 scripts to implement the general framework of the lncMod method. The first part of this framework
678 involved determining transcription factor target gene regulation specific to each cancer. Target genes
679 here are defined as any protein coding or lncRNA gene and excludes pseduogenes and small RNAs.
680 Given that ChIP-seq binding profiles for the majority of transcription factors were not available for tissues
681 associated with each of these cancers we instead used transcription factor motif analysis as a proxy. We
682 utilized motifs in the JASPAR database[88] and predictions of binding across the genome determined by
683 FIMO and available in the UCSC genome database:

684 http://expdata.cmmt.ubc.ca/JASPAR/downloads/UCSC_tracks/2018/hg19/tsv/. For each
685 transcript we determined potential regulatory transcription factors based on the presence of predicted
686 binding motifs in the gene promoter region. Promoter regions were defined as regions 3000 bp upstream
687 and downstream of the transcript's first exon. Next we selected transcription factors based on their
688 expression in each cancer and then performed linear regression considering the expression of the
689 transcription factor and target gene specific to each cancer. We adjusted the false discovery rate due to
690 multiple testing using the Benjamini-Hochberg method and selected TF-target gene pairs with
691 significantly associated expression (adjusted p-value < 1e-5).
692
693 **Identification of lncRNA modulators.** To identify transcriptional perturbation, we first delineated genes
694 (TF, target genes, or lncRNAs) that had high expression variance (IQR > 1.5). For each differentially
695 expressed lncRNA in each cancer we calculated the following, as has been done in previous
696 studies[21,22,56]. For a given cancer and given lncRNA we sorted samples in the cancer based on the given
697 lncRNAs expression (low to high). We then determined the correlation (Spearman's rho) between the
698 expression of all transcription factor and target gene pairs previously identified in the given cancer. This
699 correlation was calculated for the 25% of samples with the lowest lncRNA expression and separately for
700 the 25% of samples with the highest expression for the given lncRNA. To ensure that we observed TF-
701 target gene regulation we required that the correlation between the TF-target pair in either the low or high
702 lncRNA expressing group was at least R>0.4. We only further evaluated the lncRNA TF-target gene
703 triplet if the correlation difference between the low and high lncRNA expression group was R>0.45. To
704 formally compare the correlation difference we first normalized the correlation using the Fisher r to z
705 transformation. Then we calculated the rewiring score, z-statistic, as previously described [21], which is
706 used to describe the degree of regulation change between the TF and target gene.

707 $$F(R) = \frac{1}{2} \ln \frac{1+R}{1-R}$$

$$rewire_{TF-gene} = P\left(|X| \leq \left|\frac{F(R_{high})-F(R_{low})}{\sqrt{\frac{1.06}{n_{high}-3}+\frac{1.06}{n_{low}-3}}}\right|\right), X \sim N(0,1)$$

708

709 As a departure from what is described by Li et. al (lncMod method)[56], we used permutation analysis to
710 robustly assess the significance of the rewire score in the context of multiple hypothesis testing as
711 described by Sham et. al[89,90]. We randomly shuffled target gene expression (TF-target gene pair labels)
712 and calculated the rewire score P value across all TF-target gene pairs per given lncRNA. We kept the
713 smallest observed P value and repeated the permutation 100 times. This empirical frequency distribution
714 of the smallest P values was then compared to the P value in our real data to calculate an empirical
715 adjusted P value (adj P value) as given by the formula below, where r is the number of permutations
716 where the smallest P value are less than our actual P value and n is the number of permutations.

$$adj\ Pvalue_j = \frac{1 + (\#\ permutations\ where\ q \leq p_j)}{1 + (\#\ permutations)}$$

717

718 The lncRNA-TF-target gene triplets, with adjusted $p < 0.1$ were considered significant. Datasets with
719 smaller sample sizes had lower statistical power and thus fewer significant triplets. Triplets were then
720 classified into three patterns based on correlation changes between the low and high expressing lncRNA
721 group: increased correlation – enhanced, decreased correlation – attenuated, and inverted – positive to
722 negative correlation and vice versa. We annotated lncRNA target genes as cancer genes based on if
723 they were listed in the COSMIC database or a complied list from Chiu et. al[22].

724

725 **Cell lines and reagents.** NBL cell lines were obtained from the American Type Tissue Culture Collection
726 (ATCC) and grown in RPM1-1640 with HEPES, L-glutamine and phenol red, supplemented with 10%
727 FBS, 1% L-glutamine in an incubator at 37°C with 5% $CO_2$. Cell line identity was confirmed biennially
728 through genotyping and confirmation of STR (short tandem repeat) profiles, while routine testing for
729 Mycoplasma contamination was confirmed to be negative.

730

731 **siRNA and growth assays.** The NBL cell lines, NLF and SKNSH, were plated in a 96-well RTCES
732 microelectronic sensor array (ACEA Biosciences, San Diego, CA, USA). Cell density measurements
733 were made every hour and were normalized to 24 hours post-plating (at transfection time). We used
734 siRNAs to knockdown the expression of genes in NLF and SKNSH. The siRNAs utilized were either a
735 non-targeting negative control siRNA (Silencer™ Select Negative Control siRNA, cat #4390843), TBX2-
736 AS1 Silencer™ Select siRNA (cat # n514841), and SMARTpool: ON-TARGETplus PLK1 siRNA (cat # L-
737 003290-00-0010). Transfection of cells was done using the DharmaFECT 1 transfection reagent (cat #
738 T-2001-02). siRNA at a concentration of 50nM and 2% (NLF) and 4% (SKNSH) DharmaFECT was added
739 to RPMI medium without 10% FBS or any antibiotic separately and then incubated at room temperature
740 for 5 minutes. The siRNA medium was then added to the DharmaFECT and incubated for another 20
741 minutes to form a complex. This solution was then mixed with our normal growth media and applied to
742 cells 24 hours after they had been initially plated. All experiments were repeated in triplicate, with
743 technical replicates (n=3) being averaged per biological replicate.
744
745 **Real time quantitative PCR.** Total RNA was extracted from NBL cells using miRNeasy kit (Qiagen) and
746 the provided protocol for animal cells. The concentration of RNA was determined with the Nanodrop
747 (Thermo Scientific). cDNA synthesis was performed using the SuperScript™ First-Strand Synthesis
748 System for RT-PCR using the SuperScript™ reverse transcriptase (Invitrogen). 5-20ng of cDNA were
749 mixed with the TaqMan Universal PCR Master Mix (Thermo Fisher Scientific) and TaqMan
750 probes/primers for either TBX2-AS1 (Hs00417285_m1) or the house keeping gene, HPRT1
751 (Hs02800695_m1). Gene expression from these reactions were measured using RT-qPCR and TBX2-
752 AS1 expression was normalized to HPRT1 expression.
753
754 **NLF gene knockdown expression profiling.** Total RNA was isolated from the NLF cell line 48 hours
755 post treatment with siTBX2-AS1 and non-targeting control samples, siNTC, (three biological replicates
756 per condition) and 1000 ng/sample was used as input for library preparation with the TruSeq Stranded

757 mRNA Sample Prep Kit from Illumina (with Ribo-Zero treatment). RNA-seq libraries were sequenced on
758 the Nextseq 500 at depth 10 million reads per sample minimum. Library prep and sequencing was
759 performed by the Sidney Kimmel Cancer Center Genomics Facility of Thomas Jefferson University.
760 Sample and read quality was assessed using FastQC and reads were aligned and mapped using the
761 same methods as described above for TARGET cancer samples. Genes were retained if at least one
762 sample had expression greater than 0 FPKM. To identify differentially expressed genes between siNTC
763 and siTBX2-AS1 treated cells, we used the DESeq2 method with default parameters. Differentially
764 expressed genes were annotated based on absolute value log fold change > 1.5 and Benjamini-Hochberg
765 adjusted p-value < 0.1. Gene set enrichment analysis (GSEA) was performed across samples using the
766 MsigDB Hallmarks gene sets and significantly enriched gene sets with FDR q-val < 0.1 were retained.
767 Up-stream co-regulators of differentially expressed genes were identified using default parameters from
768 the iRegulon program part of the Cytoscape suite.
769

770 **Data Availability**
771
772 All TARGET RNA and DNA-sequencing data analyzed in this study are available through the database
773 of Genotypes and Phenotypes (dbGaP; https://www.ncbi.nlm.nih.gov/gap/) under study-id phs000218
774 and accession number phs000467. GMKF RNA-sequencing data are available through dbGAP study
775 accession phs001436.v1.p1. Neuroblastoma cell line RNA-sequencing data analyzed in this study are
776 available through GEO at accessions GSE89413. NBL histone ChIP-seq and transcription factor ChIP-
777 seq data used in this study are both available through GEO at accessions: GSE138315 and GSE94822,
778 respectively. T-ALL transcription factor ChIP-seq data and SMC1 ChIA-PET data are available through
779 GEO at accessions GSE29181, GSE59657, and GSE68977.
780
781
782 **Acknowledgements**
783
784 This work was supported in part by NIH grants R01-CA124709 (S.J.D.), R03 CA230366 (S.J.D.), X01
785 HL136997 (J.M.M.), and T32-HG46-18 (A.M.). This project was also funded in part by a supplement to

the Children's Oncology Group Chair's grant CA098543 and with federal funds from the National Cancer Institute, National Institutes of Health, under Contract No. HHSN261200800001E to S.J.D and Complete Genomics. Promoter Capture C studies were funded by the Center for Spatial and Functional Genomics (A.D.W and S.FA.G) at CHOP. S.FA.G. was supported by the Daniel B. Burke Endowed and Chair for Diabetes Research and R01 HG010067.

**Author Contributions**

A.M. and S.J.D. conceived and designed the study. M.A.S., J.M.G.A, D.S.G., E.J.P, S.M., S.P.H., S.J.D. and J.M.M. generated the TARGET data. K.L.C., M.E.J., S.J.D., A.D.W. and S.F.A.G. generated promoter-focused capture C data. E.M. C.S, and A.M. analyzed promoter-focused capture C data. A.M., G.L., S.R. analyzed TARGET data. A.M., K.L.C., T.C.L. and D.C. performed *TBX2-AS1* experiments. S.J.D. supervised the study. A.M. and S.J.D drafted the manuscript. All authors edited and approved the manuscript.

804 **References**
805
806 1. Rinn, J.L. & Chang, H.Y. Genome regulation by long noncoding RNAs. *Annu Rev Biochem* **81**,
807 145-66 (2012).
808 2. Bonasio, R. & Shiekhattar, R. Regulation of transcription by long noncoding RNAs. *Annual*
809 *review of genetics* **48**, 433-55 (2014).
810 3. Iyer, M.K. *et al.* The landscape of long noncoding RNAs in the human transcriptome. *Nature*
811 *genetics* **47**, 199-208 (2015).
812 4. Gil, N. & Ulitsky, I. Regulation of gene expression by cis-acting long non-coding RNAs. *Nat Rev*
813 *Genet* **21**, 102-117 (2020).
814 5. Dykes, I.M. & Emanueli, C. Transcriptional and Post-transcriptional Gene Regulation by Long
815 Non-coding RNA. *Genomics Proteomics Bioinformatics* **15**, 177-186 (2017).
816 6. Marchese, F.P., Raimondi, I. & Huarte, M. The multidimensional mechanisms of long noncoding
817 RNA function. *Genome Biol* **18**, 206 (2017).
818 7. Villegas, V.E. & Zaphiropoulos, P.G. Neighboring gene regulation by antisense long non-coding
819 RNAs. *International journal of molecular sciences* **16**, 3251-66 (2015).
820 8. Kopp, F. & Mendell, J.T. Functional Classification and Experimental Dissection of Long
821 Noncoding RNAs. *Cell* **172**, 393-407 (2018).
822 9. Kotake, Y. *et al.* Long non-coding RNA ANRIL is required for the PRC2 recruitment to and
823 silencing of p15(INK4B) tumor suppressor gene. *Oncogene* **30**, 1956-62 (2011).
824 10. Engreitz, J.M. *et al.* The Xist lncRNA exploits three-dimensional genome architecture to spread
825 across the X chromosome. *Science* **341**, 1237973 (2013).
826 11. Tripathi, V. *et al.* The nuclear-retained noncoding RNA MALAT1 regulates alternative splicing by
827 modulating SR splicing factor phosphorylation. *Mol Cell* **39**, 925-38 (2010).
828 12. Perry, R.B. & Ulitsky, I. The functions of long noncoding RNAs in development and stem cells.
829 *Development* **143**, 3882-3894 (2016).
830 13. Monnier, P. *et al.* H19 lncRNA controls gene expression of the Imprinted Gene Network by
831 recruiting MBD1. *Proc Natl Acad Sci U S A* **110**, 20693-8 (2013).
832 14. Lin, N. *et al.* An evolutionarily conserved long noncoding RNA TUNA controls pluripotency and
833 neural lineage commitment. *Mol Cell* **53**, 1005-19 (2014).
834 15. Yan, X. *et al.* Comprehensive Genomic Characterization of Long Non-coding RNAs across
835 Human Cancers. *Cancer Cell* **28**, 529-540 (2015).
836 16. Du, Z. *et al.* Integrative genomic analyses reveal clinically relevant long noncoding RNAs in
837 human cancer. *Nat Struct Mol Biol* **20**, 908-13 (2013).
838 17. Lanzós, A. *et al.* Discovery of Cancer Driver Long Noncoding RNAs across 1112 Tumour
839 Genomes: New Candidates and Distinguishing Features. *Scientific Reports* **7**, 1-16 (2017).
840 18. Wang, Y. *et al.* Discovery and validation of the tumor-suppressive function of long noncoding
841 RNA PANDA in human diffuse large B-cell lymphoma through the inactivation of MAPK/ERK
842 signaling pathway. *Oncotarget* **8**, 72182-72196 (2017).
843 19. Hajjari, M. & Salavaty, A. HOTAIR: an oncogenic long non-coding RNA in different cancers.
844 *Cancer Biol Med* **12**, 1-9 (2015).
845 20. Onagoruwa, O.T., Pal, G., Ochu, C. & Ogunwobi, O.O. Oncogenic Role of PVT1 and
846 Therapeutic Implications. *Front Oncol* **10**, 17 (2020).
847 21. Li, Y. *et al.* LncMAP: Pan-cancer Atlas of long noncoding RNA-mediated transcriptional network
848 perturbations. *Nucleic Acids Research* **46**, 1113-1123 (2018).
849 22. Chiu, H.S. *et al.* Pan-Cancer Analysis of lncRNA Regulation Supports Their Targeting of Cancer
850 Genes in Each Tumor Context. *Cell Rep* **23**, 297-312 e12 (2018).
851 23. Huarte, M. The emerging role of lncRNAs in cancer. *Nature medicine* **21**, 1253-61 (2015).
852 24. Xu, Y. *et al.* Identification and comprehensive characterization of lncRNAs with copy number
853 variations and their driving transcriptional perturbed subpathways reveal functional significance
854 for cancer. *Brief Bioinform* (2019).

855 25. Mondal, T. *et al.* Sense-Antisense lncRNA Pair Encoded by Locus 6p22.3 Determines
856 Neuroblastoma Susceptibility via the USP36-CHD7-SOX9 Regulatory Axis. *Cancer Cell* **33**,
857 417-434.e7 (2018).
858 26. Russell, M.R. *et al.* CASC15-S is a tumor suppressor lncRNA at the 6p22 neuroblastoma
859 susceptibility locus. *Cancer Res* **75**, 3155-3166 (2016).
860 27. Pandey, G.K. *et al.* The Risk-Associated Long Noncoding RNA NBAT-1 Controls
861 Neuroblastoma Progression by Regulating Cell Proliferation and Neuronal Differentiation.
862 *Cancer Cell* **26**, 722-737 (2014).
863 28. Sahu, D. *et al.* Co-expression analysis identifies long noncoding RNA SNHG1 as a novel
864 predictor for event-free survival in neuroblastoma. *Oncotarget* **7**, 58022-58037 (2016).
865 29. Mazar, J. *et al.* The long non-coding RNA GAS5 differentially regulates cell cycle arrest and
866 apoptosis through activation of BRCA1 and p53 in human neuroblastoma. *Oncotarget* **5**, 6589-
867 6607 (2016).
868 30. Rombaut, D. *et al.* Integrative analysis identifies lincRNAs up- and downstream of
869 neuroblastoma driver genes. *Sci Rep* **9**, 5685 (2019).
870 31. Ngoc, P.C.T. *et al.* Identification of novel lncRNAs regulated by the TAL1 complex in T-cell
871 acute lymphoblastic leukemia. *Leukemia* **32**, 2138-2151 (2018).
872 32. Trimarchi, T. *et al.* Genome-wide mapping and characterization of Notch-regulated long
873 noncoding RNAs in acute leukemia. *Cell* **158**, 593-606 (2014).
874 33. Liu, Y., Liu, H. & Zhang, D. Identification of novel long non-coding RNA in diffuse intrinsic
875 pontine gliomas by expression profile analysis. *Oncol Lett* **16**, 6401-6406 (2018).
876 34. McDaniel, L.D. *et al.* Common variants upstream of MLF1 at 3q25 and within CPZ at 4p16
877 associated with neuroblastoma. *PLoS Genet* **13**, e1006787 (2017).
878 35. Downing, J.R. *et al.* The Pediatric Cancer Genome Project. *Nat Genet* **44**, 619-22 (2012).
879 36. Ma, X. *et al.* Pan-cancer genome and transcriptome analyses of 1,699 paediatric leukaemias
880 and solid tumours. *Nature* **555**, 371-376 (2018).
881 37. Pertea, M. *et al.* StringTie enables improved reconstruction of a transcriptome from RNA-seq
882 reads. *Nature biotechnology* **33**, 290-5 (2015).
883 38. Frankish, A. *et al.* GENCODE reference annotation for the human and mouse genomes. *Nucleic*
884 *Acids Res* **47**, D766-D773 (2019).
885 39. Li, A., Zhang, J. & Zhou, Z. PLEK: a tool for predicting long non-coding RNAs and messenger
886 RNAs based on an improved k-mer scheme. *BMC Bioinformatics* **15**, 311 (2014).
887 40. Consortium, G.T. Human genomics. The Genotype-Tissue Expression (GTEx) pilot analysis:
888 multitissue gene regulation in humans. *Science* **348**, 648-60 (2015).
889 41. Yanai, I. *et al.* Genome-wide midrange transcription profiles reveal expression level
890 relationships in human tissue specification. *Bioinformatics* **21**, 650-9 (2005).
891 42. Kryuchkova-Mostacci, N. & Robinson-Rechavi, M. A benchmark of gene expression tissue-
892 specificity metrics. *Brief Bioinform* **18**, 205-214 (2017).
893 43. Dong, K., Tang, W. & Dong, R. MEG3, HCN3 and linc01105 influence proliferation and
894 apoptosis of neuroblastoma cells via HIF-1 alpha and p53 pathway. *Pediatric Blood and Cancer*
895 **63**, S194 (2016).
896 44. Lopez, G. *et al.* Somatic structural variation targets neurodevelopmental genes and identifies
897 SHANK2 as a tumor suppressor in neuroblastoma. *Genome Res* **30**, 1228-1242 (2020).
898 45. Mermel, C.H. *et al.* GISTIC2.0 facilitates sensitive and confident localization of the targets of
899 focal somatic copy-number alteration in human cancers. *Genome Biol* **12**, R41 (2011).
900 46. Pugh, T.J. *et al.* The genetic landscape of high-risk neuroblastoma. *Nat Genet* **45**, 279-84
901 (2013).
902 47. Gadd, S. *et al.* A Children's Oncology Group and TARGET initiative exploring the genetic
903 landscape of Wilms tumor. *Nat Genet* **49**, 1487-1494 (2017).

904 48. Harvey, R.C. *et al.* Identification of novel cluster groups in pediatric high-risk B-precursor acute
905 lymphoblastic leukemia with gene expression profiling: correlation with genome-wide DNA copy
906 number alterations, clinical characteristics, and outcome. *Blood* **116**, 4874-84 (2010).
907 49. Emmrich, S. *et al.* LincRNAs MONC and MIR100HG act as oncogenes in acute
908 megakaryoblastic leukemia. *Mol Cancer* **13**, 171 (2014).
909 50. Gruber, T.A. & Downing, J.R. The biology of pediatric acute megakaryoblastic leukemia. *Blood*
910 **126**, 943-9 (2015).
911 51. Liu, Y. *et al.* Genome-wide screening for functional long noncoding RNAs in human cells by
912 Cas9 targeting of splice sites. *Nat Biotechnol* (2018).
913 52. Zhao, X. *et al.* CTCF cooperates with noncoding RNA MYCNOS to promote neuroblastoma
914 progression through facilitating MYCN expression. *Oncogene*, 1-12 (2015).
915 53. Ng, S.Y., Bogu, G.K., Soh, B. & Stanton, L.W. The long noncoding RNA RMST interacts with
916 SOX2 to regulate neurogenesis. *Molecular Cell* **51**, 349-359 (2013).
917 54. Tseng, Y.Y. *et al.* PVT1 dependence in cancer with MYC copy-number increase. *Nature* **512**,
918 82-6 (2014).
919 55. Jeon, Y. & Lee, J.T. YY1 tethers Xist RNA to the inactive X nucleation center. *Cell* **146**, 119-33
920 (2011).
921 56. Li, Y. *et al.* Identification and characterization of lncRNA mediated transcriptional dysregulation
922 dictates lncRNA roles in glioblastoma. *Oncotarget* **7**, 45027-45041 (2016).
923 57. Liberzon, A. *et al.* The Molecular Signatures Database (MSigDB) hallmark gene set collection.
924 *Cell Syst* **1**, 417-425 (2015).
925 58. Delgado, M.D. & Leon, J. Myc roles in hematopoiesis and leukemia. *Genes Cancer* **1**, 605-16
926 (2010).
927 59. Amaral, P.P. *et al.* Genomic positional conservation identifies topological anchor point RNAs
928 linked to developmental loci. *Genome Biol* **19**, 32 (2018).
929 60. Wang, M. *et al.* Long noncoding RNA GAS5 promotes bladder cancer cells apoptosis through
930 inhibiting EZH2 transcription. *Cell Death Dis* **9**, 238 (2018).
931 61. Zhao, Y. *et al.* Long non-coding RNA (lncRNA) small nucleolar RNA host gene 1 (SNHG1)
932 promote cell proliferation in colorectal cancer by affecting P53. *Eur Rev Med Pharmacol Sci* **22**,
933 976-984 (2018).
934 62. Kharabi Masouleh, B. *et al.* Mechanistic rationale for targeting the unfolded protein response in
935 pre-B acute lymphoblastic leukemia. *Proc Natl Acad Sci U S A* **111**, E2219-28 (2014).
936 63. Federico, S., Brennan, R. & Dyer, M.A. Childhood cancer and developmental biology a crucial
937 partnership. *Curr Top Dev Biol* **94**, 1-13 (2011).
938 64. Cao, J. *et al.* A human cell atlas of fetal gene expression. *Science* **370**(2020).
939 65. Boeva, V. *et al.* Heterogeneity of neuroblastoma cell identity defined by transcriptional
940 circuitries. *Nat Genet* **49**, 1408-1413 (2017).
941 66. van Groningen, T. *et al.* Neuroblastoma is composed of two super-enhancer-associated
942 differentiation states. *Nat Genet* **49**, 1261-1266 (2017).
943 67. Hanzelmann, S., Castelo, R. & Guinney, J. GSVA: gene set variation analysis for microarray
944 and RNA-seq data. *BMC Bioinformatics* **14**, 7 (2013).
945 68. Signal, B., Gloss, B.S. & Dinger, M.E. Computational Approaches for Functional Prediction and
946 Characterisation of Long Noncoding RNAs. *Trends in Genetics* **32**, 620-637 (2016).
947 69. Durbin, A.D. *et al.* Selective gene dependencies in MYCN-amplified neuroblastoma include the
948 core transcriptional regulatory circuitry. *Nat Genet* **50**, 1240-1246 (2018).
949 70. Mansour, M.R. *et al.* An oncogenic super-enhancer formed through somatic mutation of a
950 noncoding intergenic element. *Science* **346**, 1373-1377 (2014).
951 71. Sanda, T. *et al.* Core transcriptional regulatory circuit controlled by the TAL1 complex in human
952 T cell acute lymphoblastic leukemia. *Cancer Cell* **22**, 209-21 (2012).

72. Verboom, K. *et al.* A comprehensive inventory of TLX1 controlled long non-coding RNAs in T-cell acute lymphoblastic leukemia through polyA+ and total RNA sequencing. *Haematologica* **103**, e585-e589 (2018).
73. Chesi, A. *et al.* Genome-scale Capture C promoter interactions implicate effector genes at GWAS loci for bone mineral density. *Nat Commun* **10**, 1260 (2019).
74. Decaesteker, B. *et al.* TBX2 is a neuroblastoma core regulatory circuitry component enhancing MYCN/FOXM1 reactivation of DREAM targets. *Nat Commun* **9**, 4866 (2018).
75. Liu, Y. *et al.* The genomic landscape of pediatric and young adult T-lineage acute lymphoblastic leukemia. *Nat Genet* **49**, 1211-1218 (2017).
76. Harenza, J.L. *et al.* Transcriptomic profiling of 39 commonly-used neuroblastoma cell lines. *Sci Data* **4**, 170033 (2017).
77. Janky, R. *et al.* iRegulon: from a gene list to a gene regulatory network using large motif and track collections. *PLoS Comput Biol* **10**, e1003731 (2014).
78. Bourdoumis, A. *et al.* The novel prostate cancer antigen 3 (PCA3) biomarker. *Int Braz J Urol* **36**, 665-8; discussion 669 (2010).
79. Slack, F.J. & Chinnaiyan, A.M. The Role of Non-coding RNAs in Oncology. *Cell* **179**, 1033-1055 (2019).
80. Chen, Y., Xu, L., Lin, R.Y., Muschen, M. & Koeffler, H.P. Core transcriptional regulatory circuitries in cancer. *Oncogene* (2020).
81. Zhang, X. & Ho, T.T. Computational Analysis of lncRNA Function in Cancer. *Methods Mol Biol* **1878**, 139-155 (2019).
82. Scheibe, M., Butter, F., Hafner, M., Tuschl, T. & Mann, M. Quantitative mass spectrometry and PAR-CLIP to identify RNA-protein interactions. *Nucleic Acids Res* **40**, 9897-902 (2012).
83. Chu, C., Qu, K., Zhong, F.L., Artandi, S.E. & Chang, H.Y. Genomic maps of long noncoding RNA occupancy reveal principles of RNA-chromatin interactions. *Mol Cell* **44**, 667-78 (2011).
84. Hon, C.C. *et al.* An atlas of human long non-coding RNAs with accurate 5′ ends. *Nature* **543**, 199-204 (2017).
85. Dobin, A. *et al.* STAR: ultrafast universal RNA-seq aligner. *Bioinformatics* **29**, 15-21 (2013).
86. Ewels, P., Magnusson, M., Lundin, S. & Kaller, M. MultiQC: summarize analysis results for multiple tools and samples in a single report. *Bioinformatics* **32**, 3047-8 (2016).
87. Upton, K. *et al.* Epigenomic profiling of neuroblastoma cell lines. *Sci Data* **7**, 116 (2020).
88. Khan, A. *et al.* JASPAR 2018: update of the open-access database of transcription factor binding profiles and its web framework. *Nucleic Acids Res* **46**, D260-D266 (2018).
89. Sham, P.C. & Purcell, S.M. Statistical power and significance testing in large-scale genetic studies. *Nat Rev Genet* **15**, 335-46 (2014).
90. Wagner, B.D., Zerbe, G.O., Mexal, S. & Leonard, S.S. Permutation-based adjustments for the significance of partial regression coefficients in microarray data analysis. *Genet Epidemiol* **32**, 1-8 (2008).

993 **FIGURE LEGENDS**
994
995 **Fig 1: Pan-pediatric transcriptome characterization.**

996 **a.** Overview of pan-pediatric cancer RNA-seq dataset and schematic of data processing and filtering.
997 Reads from RNA-seq fastq files were aligned using the STAR algorithm and then gene transcripts were
998 mapped in a guided *de novo* manner and quantified via the StringTie algorithm. Genes were considered
999 novel if they did not have transcript exon structures matching genes in the GENCODE v19 or RefSeq
1000 v74 databases. Novel genes were assigned as lncRNAs based on length >200bp and non-coding
1001 potential calculated using the PLEK algorithm. Transcripts with low expression (FPKM <1 in >80%
1002 samples) were not considered for further analysis. **b.** Pie graph showing the quantity of expressed and
1003 robustly expressed protein coding genes, GENCODE/RefSeq annotated lncRNAs, and novel lncRNAs.
1004 High confidence expressed genes are distinguished from all expressed genes. Adjoining schematic gives
1005 overview of additional data types that were integrated with transcriptome data: WGS, ChIP-seq, and
1006 chromatin capture. Listed are the analyses used to elucidate lncRNAs with functional roles in pediatric
1007 cancer. **c.** Cumulative expression plots comparing the number of lncRNAs and (**d**) protein coding genes,
1008 respectively, that constitute the total sum of gene expression (FPKM) per pediatric cancer. **e.** Percentage
1009 of total lncRNA expression (FPKM) accounted for by the union of top five expressed lncRNAs per cancer
1010 (total 11 lncRNAs).
1011
1012
1013 **Fig 2: lncRNAs exhibit tissue specific expression that can distinguish cancers.**

1014 **a.** Tissue specificity index (tau score) which ranges from 0 (ubiquitously expressed) to 1 (tissue specific)
1015 is plotted for genes across three gene types: protein coding genes, lncRNAs, and novel lncRNAs. Table
1016 shows the tau score range and mean per gene type. **b.** Number of tissue specific known and novel
1017 lncRNAs in each cancer as defined by tissue specific gene threshold: tau score > 0.8. **c.** Heatmap
1018 showing the hierarchically clustered gene expression for the top five most tissue specific lncRNAs per

1019 cancer, ranked by highest tau score. Samples from each cancer cluster together based on expression of
1020 these genes alone.
1021
1022
1023 **Fig 3: A similar proportion of lncRNAs and protein coding genes are dysregulated due to SCNA**
1024 **a.** The proportion of protein coding and lncRNA genes that have significant differential expression due
1025 SCNA, separated by copy number type (amplification or deletion). The number of genes found in SCNA
1026 loci is shown per cancer. Genes were evaluated to have differential expression due to copy number using
1027 the Wilcoxon rank sum test (p-value < 0.05) and log |fold change| > 1.5), comparing samples with no
1028 SCNA to samples with low/high SCNA as defined by GISTIC scores. **b.** The number of differentially
1029 expressed lncRNAs per chromosome and per cancer, distinguished by color. Chromosome 1 and 17 had
1030 the most dysregulated lncRNAs associating with the greater frequency of SCNA on these chromosomes
1031 across cancers. **c.** Number of samples with structural variant breakpoints in or near (+/- 2.5kb) lncRNAs
1032 and that are also located in copy number regions, stratified by amplification or deletion status of the locus.
1033
1034
1035 **Fig 4: lncRNA modulators impact transcriptional networks involving proliferation.**
1036 **a.** Schematic that shows the three ways (attenuate, enhance, or invert) in which differentially expressed
1037 lncRNA modulators can impact transcription factor and target gene relationships. lncRNA modulators are
1038 associated with a TF-target gene pair based on a significant difference between TF-target gene
1039 expression correlation in samples with low lncRNA expression (lowest quartile) vs samples with high
1040 lncRNA expression (highest quartile). **b.** The proportion of lncRNA modulator types associated with
1041 significantly dysregulated lncRNA modulator- TF-target gene (lncMod) triplets. The number of
1042 significantly dysregulated lncMod triplets is listed per cancer. **c.** Number of lncRNA modulators genes
1043 that are common in lncMod triplets across cancers. Common lncRNA modulator genes tend to have a
1044 lower tau score compared to lncRNA modulators only associated with one cancer. **d.** Gene set

1045 enrichment using the MSigDB Hallmark gene set, of target genes associated with lncRNA modulators in
1046 each cancer (Fisher's exact test, FDR < 0.1). **e.** Transcription factors associated with the B-ALL
1047 expression specific lncRNA, *BLACE*, ranked based on number of regulated target genes. **f.** Expression
1048 heatmap of *BLACE* and the target genes of the XBP1 transcription factor, grouped by associated hallmark
1049 gene set, in samples within the bottom and top quartiles of *BLACE* expression in B-ALL.
1050
1051
1052 **Fig 5: Identification of lncRNAs associated with distinct neuroblastoma cell states**
1053 **a.** The MES and ADRN signature score for TARGET NBL samples, with each sample labeled with either
1054 ADRN, Mixed, or MES phenotype based on clustering analysis. **b.** Heatmap of the expression of lncRNAs
1055 that have significant correlation with either the MES or ADRN score (|r| >0.6, pval < 0.01). lncRNAs were
1056 correlated with protein coding genes on the same chromosome and subsequent gene set enrichment
1057 analysis was performed for MES and ADRN protein coding genes separately. **c.** Schematic of how ADRN
1058 associated CRC regulated genes are identified using ChIP-seq and chromatin interaction data. We
1059 identified lncRNAs based on three types of regulation. 1) CRC transcription factors binding directly at the
1060 promoter of the lncRNA. 2) CRC TFs bind an enhancer region that interacts with a lncRNA promoter. 3)
1061 CRC TFs bind the promoter of a different gene and this promoter interacts with a lncRNA promoter. CRC
1062 TF binding was identified from ChIP-seq data, while enhancer-promoter and promoter-promoter
1063 interactions were identified from chromatin capture data. **d.** Filtering of lncRNAs expressed in NBL based
1064 on CRC TF regulation and differential expression based on sample phenotypes (ADRN or MES). **e.**
1065 Expression of *TBX2* and *TBX2-AS1* stratified by NBL sample phenotype (ADRN or MES). **f.** ChIP-seq
1066 tracks for histone marks and CRC transcription factors in the NBL cell line: BE(2)C, and promoter capture
1067 C chromatin interactions in NBL cell line: NB1643, at the *TBX2*/*TBX2-AS1* locus.
1068
1069
1070 **Fig 6: The *TBX2-AS1* lncRNA plays a role in neuroblastoma proliferation by modulating TBX2**

1071 **a.** Expression of *TBX2* and *TBX2-AS1* in NBL tumor samples with and without 17q gain. **b.** The top
1072 MSigDB Hallmarks enriched across targets genes (p-value < 0.01) regulated by *TBX2-AS1* as predicted
1073 from lncMod analysis. **c.** The transcription factors with most target genes regulated by *TBX2-AS1* as
1074 predicted from lncMod analysis. **d.** Expression of gene targets of the E2F1 transcription factor that are
1075 enriched for proliferation hallmarks, in samples with low and high *TBX2* and *TBX2-AS1* expression. *TBX2*
1076 expression is highly correlated with that of *TBX2-AS1* (Pearson's r=0.77). **e.** siRNA knockdown efficiency
1077 of *TBX2-AS1* in the NBL cell line: NLF is 91% and in the SKNSH cell 63% knockdown was achieved. **f.**
1078 Western blot analysis of TBX2 in siTBX2 and siTBX2-AS1 treated NLF and SKNSH cell lines. **g.**
1079 Representative image of cell growth (as measured by RT-Ces assay) of the NBL cell lines: NLF and **h**.
1080 SKNSH. Cell index is normalized to time point when siRNA reagent is added at 24 hours post cell plating.
1081 **i.** Results from iRegulon analysis for genes that are up- or down-regulated upon siTBX2-AS1 treatment
1082 in NLF. Number of genes shown in Venn diagram with evidence of motif or ChIP-seq binding of the listed
1083 transcription factors.

# Figure 1

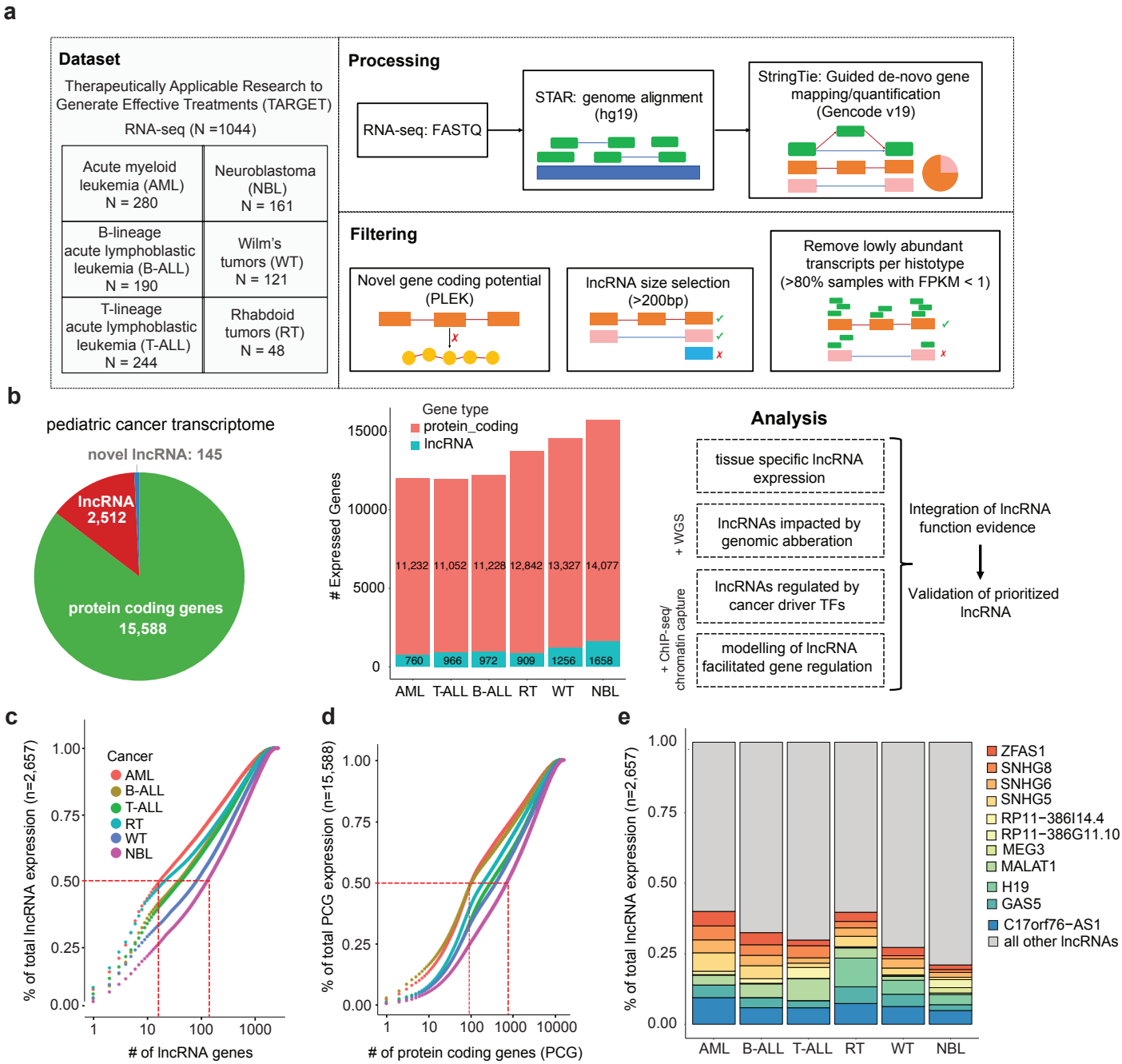


**Fig 1: Pan-pediatric transcriptome characterization.**
**a.** Overview of pan-pediatric cancer RNA-seq dataset and schematic of data processing and filtering. Reads from RNA-seq fastq files were aligned using the STAR algorithm and then gene transcripts were mapped in a guided *de novo* manner and quantified via the StringTie algorithm. Genes were considered novel if they did not have transcript exon structures matching genes in the GENCODE v19 or RefSeq v74 databases. Novel genes were assigned as lncRNAs based on length >200bp and non-coding potential calculated using the PLEK algorithm. Transcripts with low expression (FPKM <1 in >80% samples) were not considered for further analysis. **b.** Pie graph showing the quantity of expressed and robustly expressed protein coding genes, GENCODE/RefSeq annotated lncRNAs, and novel lncRNAs. High confidence expressed genes are distinguished from all expressed genes. Adjoining schematic gives overview of additional data types that were integrated with transcriptome data: WGS, ChIP-seq, and chromatin capture. Listed are the analyses used to elucidate lncRNAs with functional roles in pediatric cancer. **c.** Cumulative expression plots comparing the number of lncRNAs and (**d**) protein coding genes, respectively, that constitute the total sum of gene expression (FPKM) per pediatric cancer. **e.** Percentage of total lncRNA expression (FPKM) accounted for by the union of top five expressed lncRNAs per cancer (total 11 lncRNAs).

# Figure 2

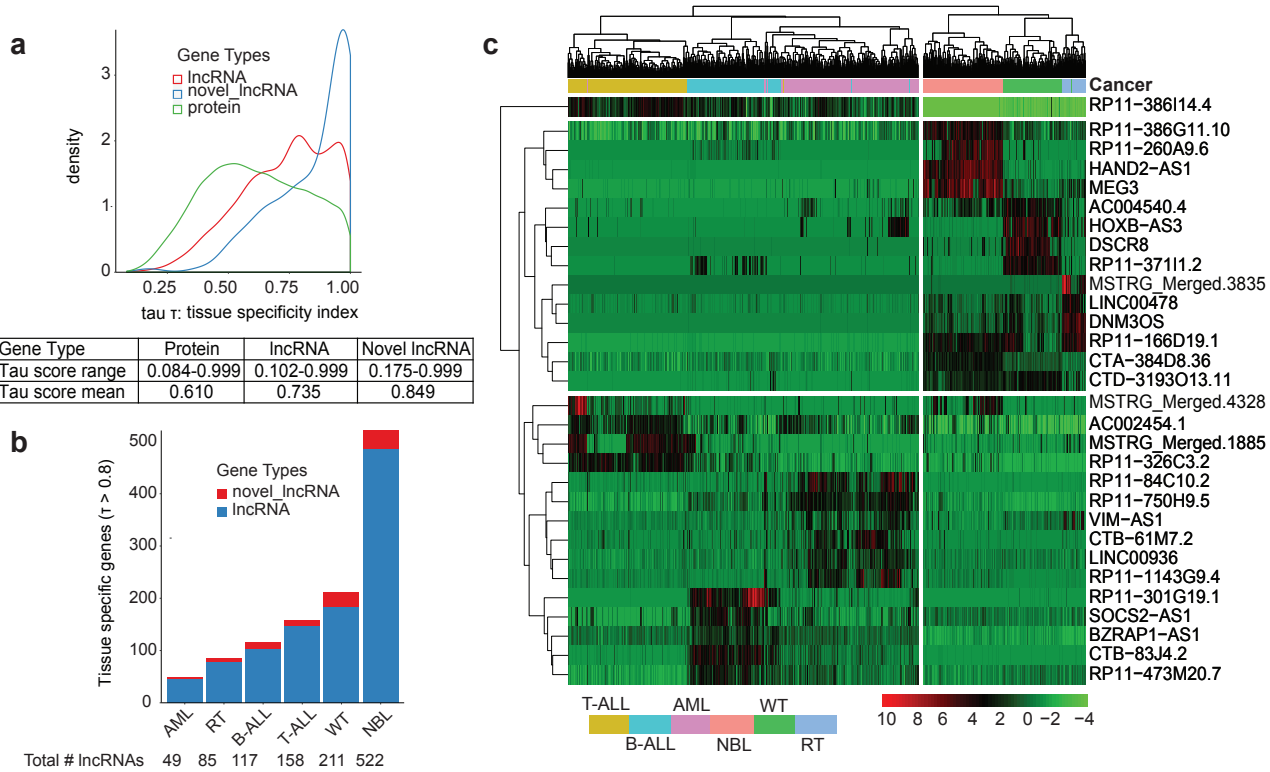


| Gene Type | Protein | lncRNA | Novel lncRNA |
|---|---|---|---|
| Tau score range | 0.084-0.999 | 0.102-0.999 | 0.175-0.999 |
| Tau score mean | 0.610 | 0.735 | 0.849 |

**Fig 2: lncRNAs exhibit tissue specific expression that can distinguish cancers.**
**a.** Tissue specificity index (tau score) which ranges from 0 (ubiquitously expressed) to 1 (tissue specific) is plotted for genes across three gene types: protein coding genes, lncRNAs, and novel lncRNAs. Table shows the tau score range and mean per gene type. **b.** Number of tissue specific known and novel lncRNAs in each cancer as defined by tissue specific gene threshold: tau score > 0.8. **c.** Heatmap showing the hierarchically clustered gene expression for the top five most tissue specific lncRNAs per cancer, ranked by highest tau score. Samples from each cancer cluster together based on expression of these genes alone.

# Figure 3

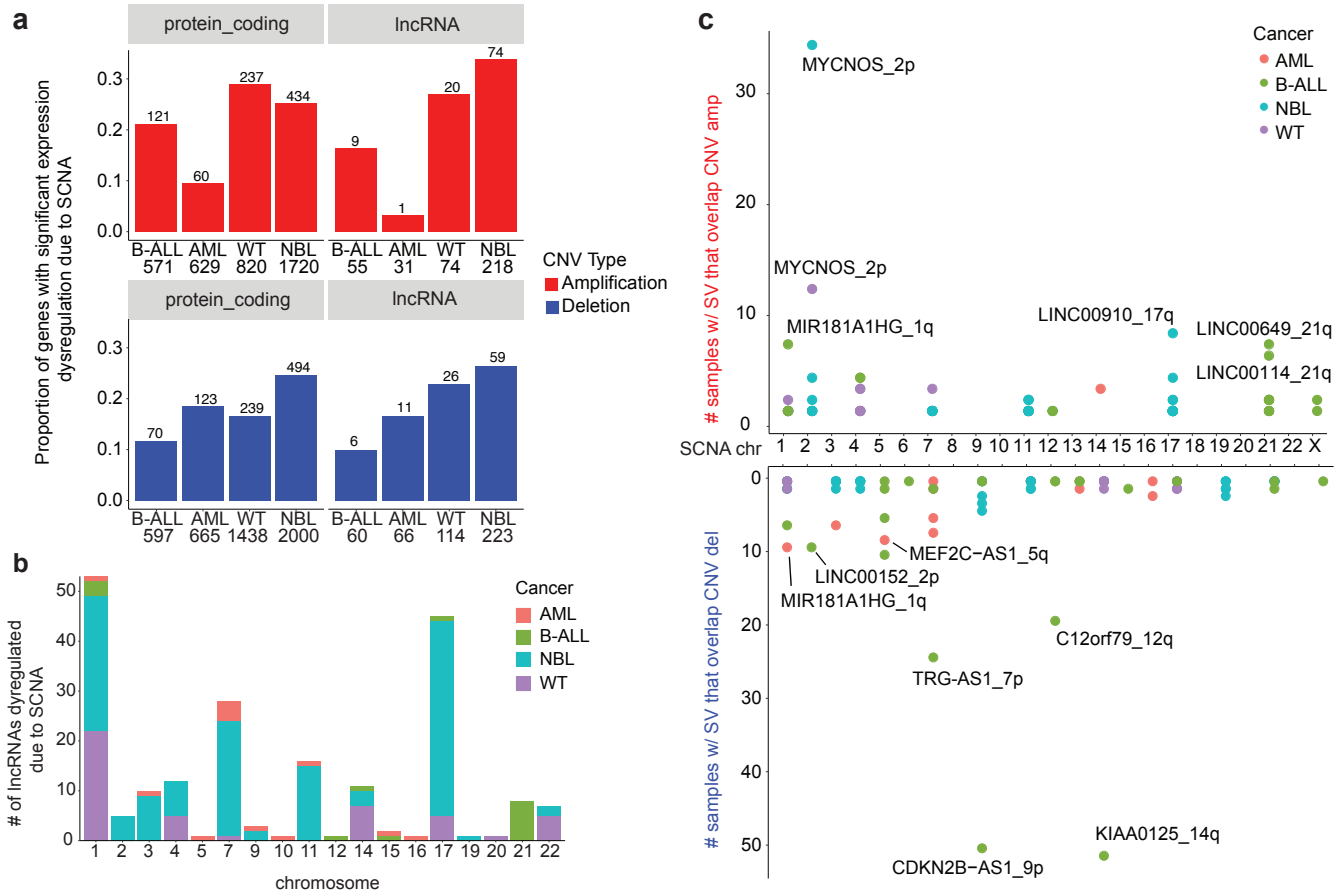


**Fig 3: A similar proportion of lncRNAs and protein coding genes are dysregulated due to SCNA**

**a.** The proportion of protein coding and lncRNA genes that have significant differential expression due SCNA, separated by copy number type (amplification or deletion). The number of genes found in SCNA loci is shown per cancer. Genes were evaluated to have differential expression due to copy number using the Wilcoxon rank sum test (p-value < 0.05) and log |fold change| > 1.5), comparing samples with no SCNA to samples with low/high SCNA as defined by GISTIC scores. **b.** The number of differentially expressed lncRNAs per chromosome and per cancer, distinguished by color. Chromosome 1 and 17 had the most dysregulated lncRNAs associating with the greater frequency of SCNA on these chromosomes across cancers. **c.** Number of samples with structural variant breakpoints in or near (+/- 2.5kb) lncRNAs and that are also located in copy number regions, stratified by amplification or deletion status of the locus.

# Figure 4

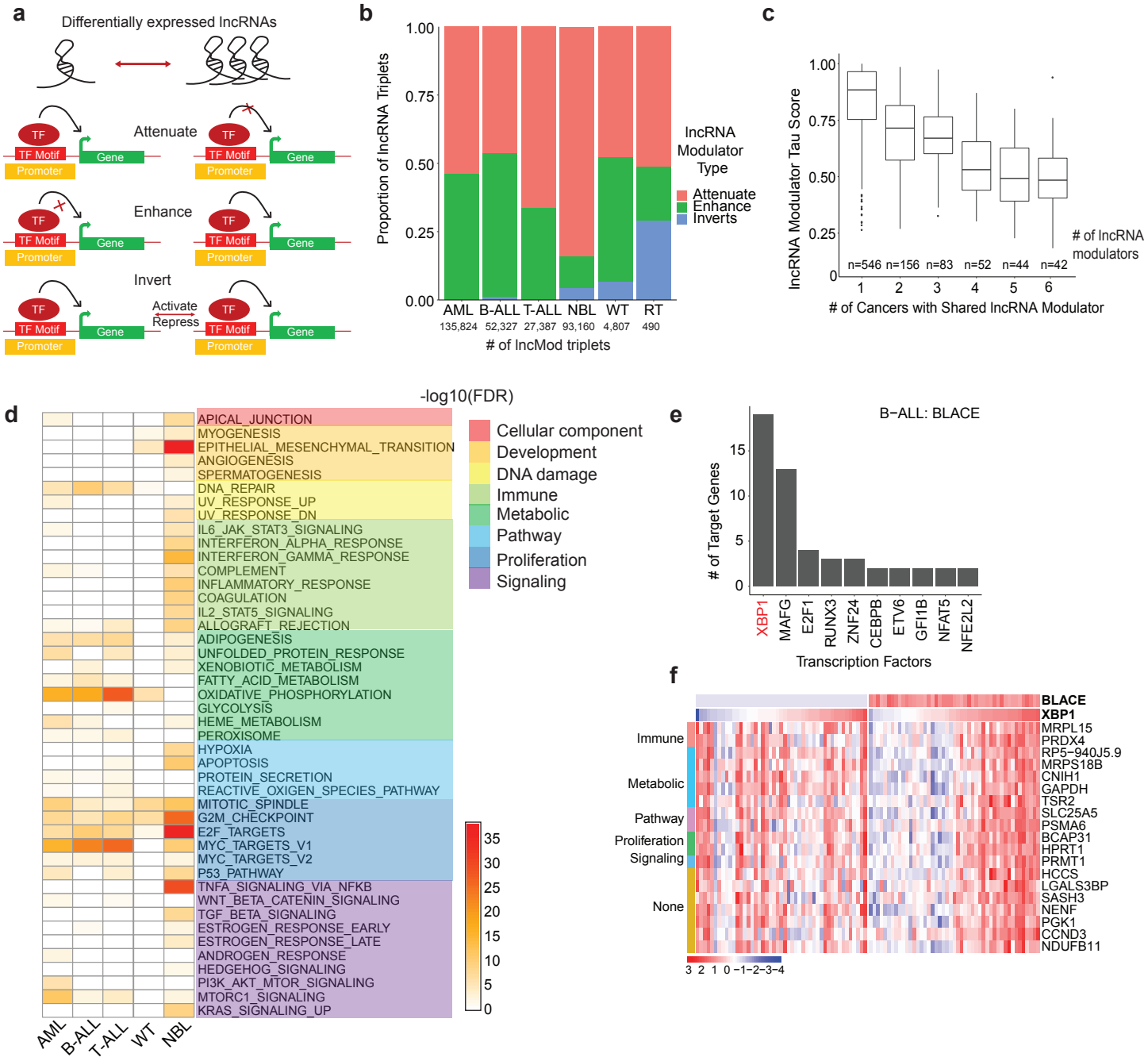


**Fig 4: lncRNA modulators impact transcriptional networks involving proliferation.** **a.** Schematic that shows the three ways (attenuate, enhance, or invert) in which differentially expressed lncRNA modulators can impact transcription factor and target gene relationships. lncRNA modulators are associated with a TF-target gene pair based on a significant difference between TF-target gene expression correlation in samples with low lncRNA expression (lowest quartile) vs samples with high lncRNA expression (highest quartile). **b.** The proportion of lncRNA modulator types associated with significantly dysregulated lncRNA modulator- TF-target gene (lncMod) triplets. The number of significantly dysregulated lncMod triplets is listed per cancer. **c.** Number of lncRNA modulators genes that are common in lncMod triplets across cancers. Common lncRNA modulator genes tend to have a lower tau score compared to lncRNA modulators only associated with one cancer. **d.** Gene set enrichment using the MSigDB Hallmark gene set, of target genes associated with lncRNA modulators in each cancer (Fisher's exact test, FDR < 0.1). **e.** Transcription factors associated with the B-ALL expression specific lncRNA, *BLACE*, ranked based on number of regulated target genes. **f.** Expression heatmap of *BLACE* and the target genes of the XBP1 transcription factor, grouped by associated hallmark gene set, in samples within the bottom and top quartiles of *BLACE* expression in B-ALL.

# Figure 5

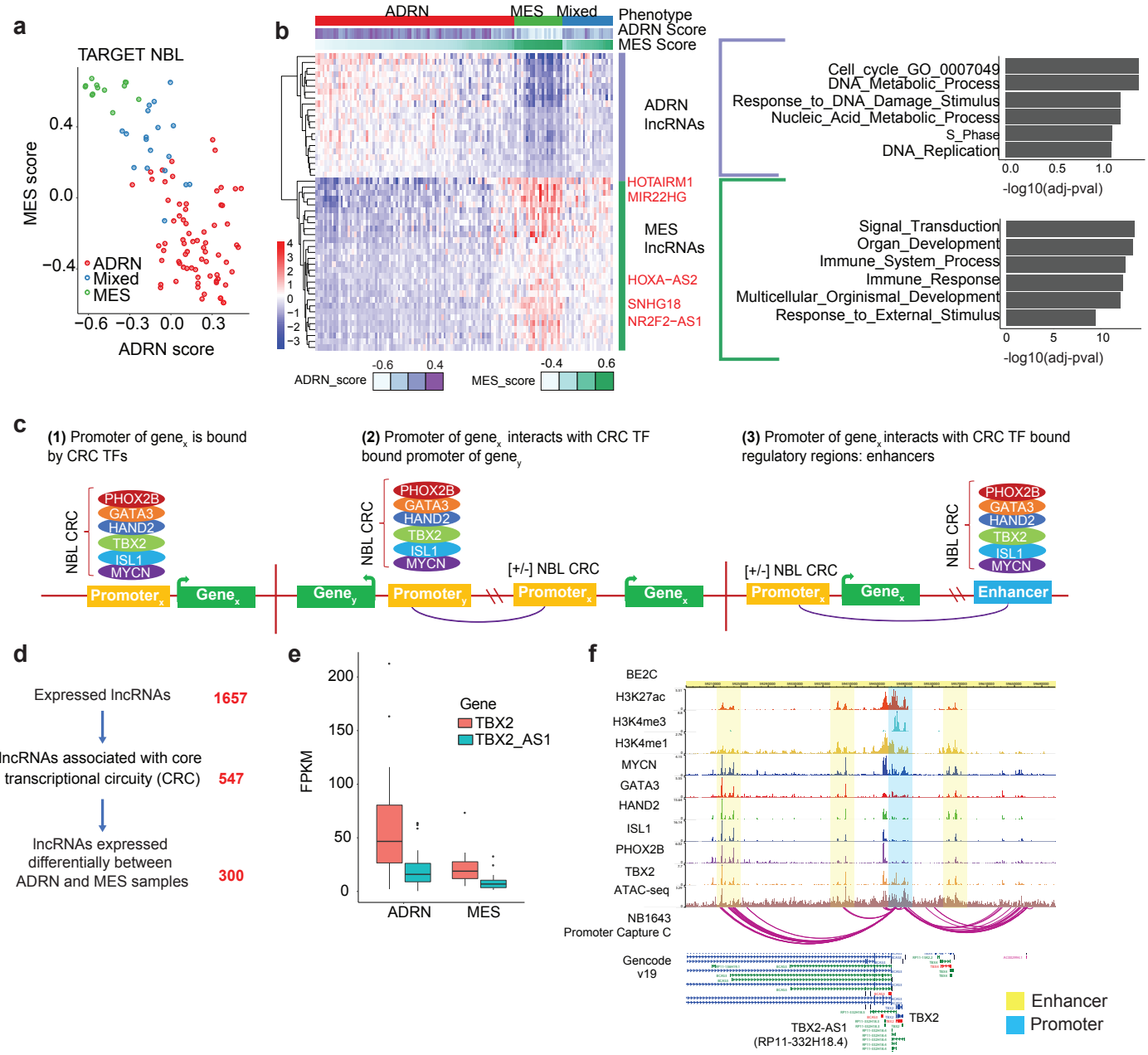


**Fig 5: Identification of lncRNAs associated with distinct neuroblastoma cell states**
**a.** The MES and ADRN signature score for TARGET NBL samples, with each sample labeled with either ADRN, Mixed, or MES phenotype based on clustering analysis. **b.** Heatmap of the expression of lncRNAs that have significant correlation with either the MES or ADRN score (|r| >0.6, pval < 0.01). lncRNAs were correlated with protein coding genes on the same chromosome and subsequent gene set enrichment analysis was performed for MES and ADRN protein coding genes separately. **c.** Schematic of how ADRN associated CRC regulated genes are identified using ChIP-seq and chromatin interaction data. We identified lncRNAs based on three types of regulation. 1) CRC transcription factors binding directly at the promoter of the lncRNA. 2) CRC TFs bind an enhancer region that interacts with a lncRNA promoter. 3) CRC TFs bind the promoter of a different gene and this promoter interacts with a lncRNA promoter. CRC TF binding was identified from ChIP-seq data, while enhancer-promoter and promoter-promoter interactions were identified from chromatin capture data. **d.** Filtering of lncRNAs expressed in NBL based on CRC TF regulation and differential expression based on sample phenotypes (ADRN or MES). **e.** Expression of *TBX2* and *TBX2-AS1* stratified by NBL sample phenotype (ADRN or MES). **f.** ChIP-seq tracks for histone marks and CRC transcription factors in the NBL cell line: BE(2)C, and promoter capture C chromatin interactions in NBL cell line: NB1643, at the *TBX2*/*TBX2-AS1* locus.

# Figure 6

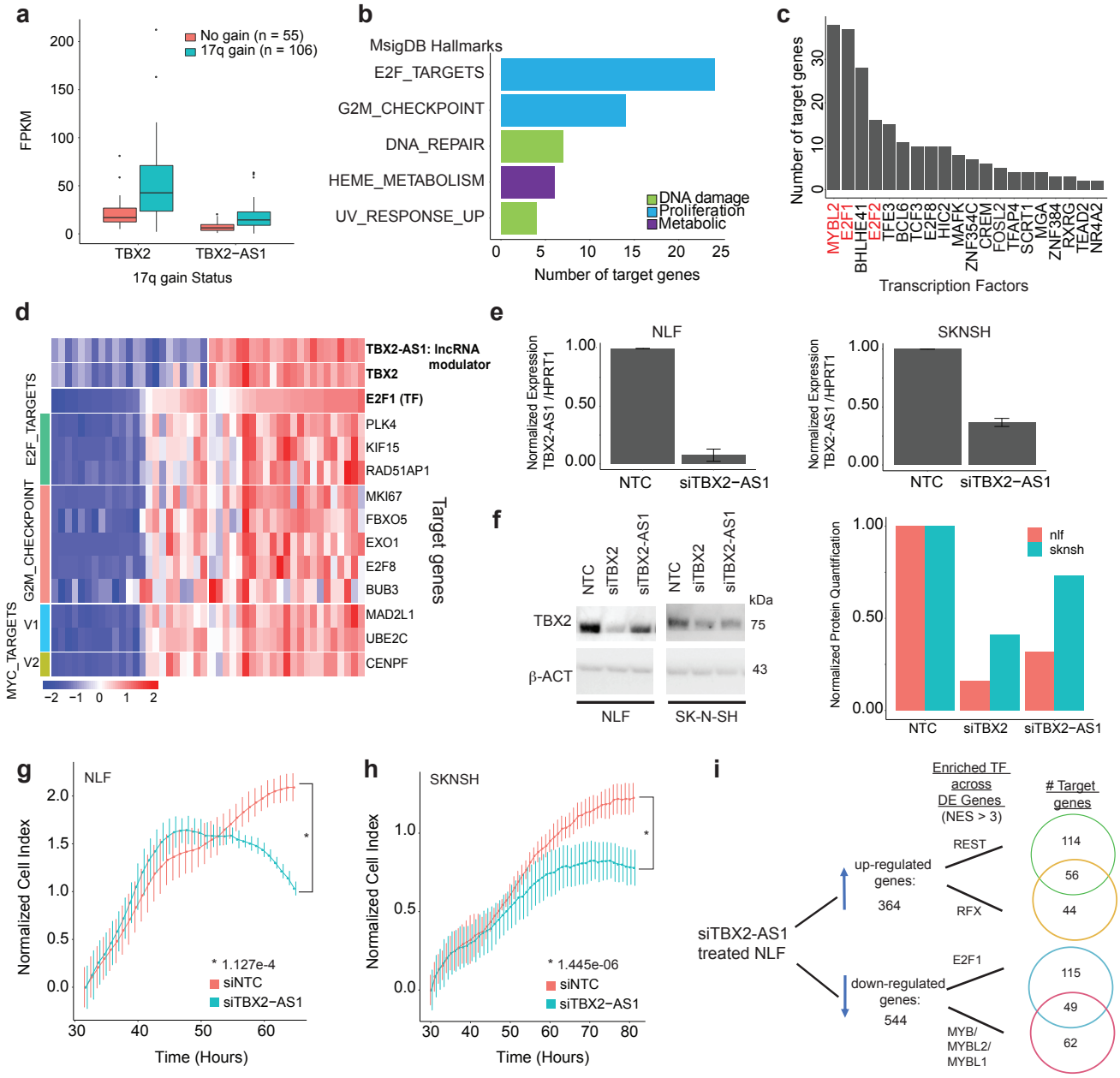


**Fig 6: The *TBX2-AS1* lncRNA plays a role in neuroblastoma proliferation by modulating TBX2**

**a.** Expression of *TBX2* and *TBX2-AS1* in NBL tumor samples with and without 17q gain. **b.** The top MSigDB Hallmarks enriched across targets genes (p-value < 0.01) regulated by *TBX2-AS1* as predicted from lncMod analysis. **c.** The transcription factors with most target genes regulated by *TBX2-AS1* as predicted from lncMod analysis. **d.** Expression of gene targets of the E2F1 transcription factor that are enriched for proliferation hallmarks, in samples with low and high *TBX2* and *TBX2-AS1* expression. *TBX2* expression is highly correlated with that of *TBX2-AS1* (Pearson's r=0.77). **e.** siRNA knockdown efficiency of *TBX2-AS1* in the NBL cell line: NLF is 91% and in the SKNSH cell 63% knockdown was achieved. **f.** Western blot analysis of TBX2 in siTBX2 and siTBX2-AS1 treated NLF and SKNSH cell lines. **g.** Representative image of cell growth (as measured by RT-Ces assay) of the NBL cell lines: NLF and **h**. SKNSH. Cell index is normalized to time point when siRNA reagent is added at 24 hours post cell plating. **i.** Results from iRegulon analysis for genes that are up- or down-regulated upon siTBX2-AS1 treatment in NLF. Number of genes shown in Venn diagram with evidence of motif or ChIP-seq binding of the listed transcription factors.